Master's thesis

2019

Ragnhild Sofie Ragnhildstveit Sætra

NTNU
Norwegian University of
Science and Technology
Faculty of Medicine and Health Sciences
Department of Clinical and Molecular Medicine

Ragnhild Sofie Ragnhildstveit Sætra

Membrane damage and inflammasome activation during *Mtb* infection

June 2019

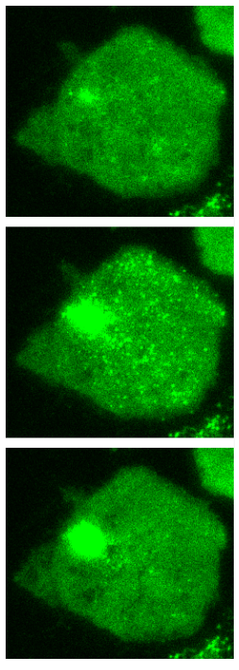

NTNU
Norwegian University of
Science and Technology

NTNU
Norwegian University of
Science and Technology

NTNU
Norwegian University of
Science and Technology

Membrane damage and inflammasome activation during *Mtb* infection

Ragnhild Sofie Ragnhildstveit Sætra

Nanotechnology
Submission date: June 2019
Supervisor: Kai Sandvold Beckwith

Norwegian University of Science and Technology
Department of Clinical and Molecular Medicine

Preface

This thesis describes work conducted in the spring semester 2019 and is submitted as part of the requirements for the degree of Master of Science at the Norwegian University of Science and Technology (NTNU). This concludes the 5-year MTNANO program of study with a specialization in bionanotechnology. The work has been conducted at the Center for Molecular Inflammatory Research (CEMIR), with post.doc. Kai Sandvold Beckwith as supervisor.

The reader should be familiar with basic cell biology and immunology, although an introduction to the theoretical background for the project will be given.

The work described herein is a continuation of experiments conducted and reported through a project report in the fall semester of 2018. Parts of the theory section therefore bear similarity to the project report, but have been rewritten. A short summary of the findings in the project work can be found in the introduction section. Unless otherwise stated, all figures in this thesis are made by the author.

There are several people that deserve appreciation for helping me during my time as a Master's student. First of all, I would like to thank my supervisor, Kai Sandvold Beckwith. His great insight, many ideas and positive attitude has been both inspiring and very helpful.

While working on this topic, I have been a part of the research group Molecular Mechanisms of Mycobacterial and HIV Infections, led by Professor Trude Helen Flo. I am grateful to all group members for always answering questions I have had along the way. Especially I would like to thank Trude for welcoming me to the group. Thank you also to Haelin, for making this year so much fun, and to Sindre, for giving me feedback and for introducing me to Kai. Thank you to Bjørnar Sporsheim and Kjartan Wøllo Egeberg at CMIC for always helping me whenever I had issues with the microscope.

I would also like to thank my friends from the MTNANO program for all the fun we have had along the way – they made these five years of studying a pleasure.

Finally, I would like to thank Anders Strømberg for always being there for me, no matter the stress level.

Trondheim, June 11, 2019

Ragnhild Sofie Ragnhildstveit Sætra

Abstract

Tuberculosis, which is caused by *Mycobacterium tuberculosis* (*Mtb*), is a global health problem, and understanding the molecular mechanisms of *Mtb* infection is therefore important. On a single-cell level, *Mtb* infection can result in activation of the NLRP3 inflammasome, and damage to the plasma membrane might be important in driving this. A set of proteins known as ESCRT has in the recent years emerged as important for plasma membrane repair, and could thus have a role in this system. Furthermore, autophagy targets *Mtb* when the bacterium escapes into the cytosol, and possibly also impacts the outcome.

The work described in this thesis aimed to discover new details about the molecular interplay between phagosomal escape, autophagy and membrane repair during NLRP3 inflammasome activation and mycobacterial infection. Total internal reflection fluorescence (TIRF) microscopy on live THP-1 cells was used to address this. Cells expressing fluorescently labeled proteins were infected with the auxotroph *Mtb* $mc^2$6206, and observed with TIRF microscopy. The results were compared to those obtained from treating the cells with nanosilica, a known NLRP3 trigger through lysosomal disruption. Furthermore, the fluorescent dye Calbryte 590 AM was used to assess the role of calcium fluxes in the system.

It was found that subsequent to phagosomal escape, identified by recruitment of galectin 3 (gal3), the ESCRT-associated protein ALG2 was frequently recruited to the plasma membrane. About half of the ALG2 plasma membrane recruitment events could be seen to be located at the site of a gal3-positive compartment. This recruitment correlated with a calcium influx to the cytosol. Autophagy machinery was to a greater degree recruited to gal3-positive compartments that were unrelated to ALG2 plasma membrane recruitment events. Autophagy could thus be a negative regulator of the process. However, delaying the autophagy onset did not affect ALG2.

These results support that NLRP3 triggers that damage lysosomal compartments share a common mechanism of a calcium influx. Furthermore, *Mtb* infection is contained by ESCRT, which repairs damage inflicted by the bacterium upon the plasma membrane. This plasma membrane damage could be the driver of NLRP3 activation. These findings are both interesting for understanding of the molecular mechanisms of *Mtb*, and for diseases related to dysfunctional NLRP3.

Sammendrag

Tuberkulose, som forårsakes av *Mycobacterium tuberculosis* (*Mtb*), er et globalt helseproblem, og økt forståelse av de molekylære mekanismene bak *Mtb*-infeksjon er viktig. På enkeltcellenivå kan *Mtb*-infeksjon føre til aktivering av NLRP3-inflammasomet, og skade på plasmamembranen kan være en drivkraft bak dette. Proteinsystemet ESCRT har de siste årene vist seg å være viktig i plasmamembranreparasjon, og kan dermed ha en rolle i dette systemet. I tillegg kan autofagimaskineri rekrutteres til *Mtb* når bakterien er fri i cytosol. Autofagi kan derfor også påvirke utfallet.

Arbeidet som beskrives i denne masteroppgaven hadde som målsetning å avdekke nye detaljer om det molekylære samspillet mellom fagosomal rømning, autofagi og membranreparasjon under NLRP3-inflammasomaktivering og mykobakteriell infeksjon. Total intern refleksjon-fluorescensmikroskopi (TIRF-mikroskopi) på levende THP-1-celler ble benyttet for å undersøke dette. Celler som uttrykte fluorescensmerkede proteiner ble infisert med auxotrofen *Mtb* $mc^2$6206, og deretter studert med TIRF-mikroskopi. Resultatene ble sammenliknet med resultater fra behandling av cellene med nanosilica, som er en kjent NLRP3-trigger via lysosomødeleggelse. Videre ble det fluorescente fargestoffet Calbryte 590 AM brukt til å undersøke rollen til kalsiumflukser.

Resultatene viste at etter bakterien fikk tilgang til cytosol, identifisert ved rekruttering av galectin 3 (gal3), kunne man ofte se rekruttering av det ESCRT-assosierte proteinet ALG2 til plasmamembranen. Omtrent halvparten av ALG2-rekrutteringshendelsene skjedde på samme sted som en gal3-positiv membranlomme. Denne rekrutteringen korrelerte med kalsiumtilstrømning i cytosol. Autofagimaskineri ble i større grad rekruttert til gal3-positive membranlommer som ikke var relatert til plasmamembranrekruttering av ALG2. Autofagi kan altså være en negative regulator av prosessen. Inhibering av autofagi resulterte imidlertid ikke i noen endring I ALG2-mønsteret.

Disse resultatene støtter at NLRP3-triggere som utøver lysosomskade har kalsiumtilstrømning som en fellesnevner. Videre sees det at *Mtb*-infeksjon kontrolleres av ESCRT, som forsøker å reparere bakterie-mediert skade på plasmamembranen. Denne plasmamembranskaden kan være en drivkraft for NLRP3-aktivering. Disse funnene er interessante i flere kontekster – både for å forstå de molekylære mekanismene bak *Mtb*-infeksjon, og for å forstå sykdommer relatert til dysfunksjonell NLRP3.

List of abbreviations

Mtb	*Mycobacterium tuberculosis*
RD1	Region of difference 1
ESAT-6	Early secreted antigenic target of 6 kDa
ESX-1	ESAT-6 secretion system 1
PAMP	Pathogen-associated molecular pattern
DAMP	Damage-associated molecular pattern
PRR	Pathogen-recognition receptor
Gal3	Galectin 3
NOD	Nuceotide oligomerization domain
NLR	NOD-like receptor
CARD	Caspase activation and recruitment domain
ASC	Apoptosis-associated speck-like protein containing a CARD
TLR	Toll-like receptor
ROS	Reactive oxygen species
GSDMD	Gasdermin D
ESCRT	Endosomal sorting complex required for transport
ALG2	Apoptosis-linked gene 2
ALIX	ALG2 interacting protein X
ULK1	Unc-1-like kinase 1
mTOR	Mammalian target of rapamycin
AMPK	AMP-activated protein kinase
LC3	Microtubule-associaed proteins 1A/1B light chain 3
LAP	LC3-associated phagocytosis
TIRF	Total internal reflection fluorescence
OD	Optical density
ROI	Region of interest

Contents

Chapter 1

Introduction

This introduction chapter will provide the reader with an overview of the background and motivation which create the foundation for the project work. Numbers and facts relating to tuberculosis are retrieved from the *Global tuberculosis report 2018* by the World Health Organization [1], unless otherwise stated. Furthermore, an overview of the aim and methodology of the work will be provided.

1.1 Motivation and background

Tuberculosis has been plaguing mankind for thousands of years. This single disease alone has been the leading cause of death in several European countries in the past, although in recent years, its grave and fatal nature is often considered an outdated problem. Despite this public perception, however, 10 million people still develop the disease every year, and tuberculosis is one of the top ten leading causes of death in the world. Furthermore, it is estimated that 1.7 billion people have a latent tuberculosis infection, and could therefore develop active disease later in life.

In the late 1800s, it was discovered that tuberculosis is caused by the microbe *Mycobacterium tuberculosis (Mtb)*. Ever since, the battle between the human immune system and this bacterium has been a growing topic of research. Tuberculosis is considered curable, commonly achieved through a burdensome 6-month antibiotics cure. However, drug-resistant tuberculosis is a growing issue: Over half a million people developed this form of the disease in 2017, out of which 82% of the cases were considered multidrug-resistant. In these forms of tuberculosis, treatment is more complicated and has lower success rates. Evidently, new approaches to therapy could be a necessity, and in order to develop these, a thorough understanding of the disease on a molecular level is needed. Furthermore, such knowledge is needed to develop

better vaccines for prevention of tuberculosis, and could aid in the field of diagnostics as well, contributing towards total eradication of the disease.

Mtb is spread between hosts through air: One infected individual coughs or sneezes, and a healthy individual breathes in aerosol that contains the bacterium. Once the bacterium reaches the lungs, alveolar macrophages recognize it as dangerous. This type of cells are a crucial part of the innate immune system, the first line of defense. Their main task is to recognize, ingest and eliminate substances that are sensed to be dangerous, a process known as *phagocytosis*. To eliminate the threat, the macrophages therefore phagocytose and try to digest the microbe. However, *Mtb* manages to stay alive within cells, stopping the maturation of their residing compartment into a bactericidal milieu [2]. This mechanism is crucial for successful infection.

A key virulence factor for *Mycobacterium tuberculosis* has been discovered to be the genetic locus region of difference 1 (RD1), which encodes the *early secreted antigenic target of 6 kDa* (ESAT-6) secretion system 1 (ESX-1) [3]. Using this system, the bacterium manages to breach the phagosomal membrane that encapsulates it, and thereby gain access to the cytosol of the host.

When the bacterium is free in the cytosol, either partly or completely, other host mechanisms come into play. The autophagy machinery often sense the bacterium under these conditions, and try to digest it as a measure to limit the spread of the pathogen [4]. Also, the NLRP3 inflammasome, a large immunological signaling platform, can be activated once bacterial products are free in the cytosol [5]. As a result of this activation, the signaling molecule IL-1β can be processed into its mature form, and released into the extracellular environment, where it exerts pro-inflammatory functions by binding to extracellular receptors. These effects include increased expression of inflammatory molecules, and recruitment and activation of other immune cells [6]. Furthermore, as disruption of membranes is central to the virulence of *Mtb*, membrane repair during infection is interesting to examine. An emerging new player here is the ESCRT system, which has been shown to aid in the repair of plasma membrane wounds [7].

The cellular processes that occur during infection can be studied in several ways. Direct, single-cell observation of these events is for instance made possible through fluorescence microscopy. In this technique, quantum mechanical energy transitions are utilized to visualize proteins, organelles or other features in the cell, labeled by chemical or genetic tools. Furthermore, by examining only a few cells at the time, one is able to assess the heterogeneity of cellular processes.

1.2 Aim of work

This thesis presents work aimed at elucidating the interplay between phagosomal escape, plasma membrane damage and inflammasome activation elicited by infection with *Mtb*. The THP-1 cell line was used as a macrophage model, and the auxotroph *Mtb* $mc^2$6206 mimicked *Mtb*. The cellular responses were compared to those appearing during treatment with nanosilica, which activates the NLRP3 inflammasome through disrupting lysosomal function. The employed method for examining these responses has been TIRF fluorescence microscopy, which enables plasma membrane-sensitive detection of events, as well as widefield fluorescence microscopy.

The work described herein is a continuation of experiments conducted during the fall of 2018, which were summarized in a project report [8]. Briefly, this project concerned mechanisms of NLRP3 inflammasome activation. It was found that ALG2, a protein associated with the ESCRT membrane repair system, was recruited to the plasma membrane immediately after ASC speck formation. This process was suspected to be mediated by GSDMD pores. When using potassium-dependent NLRP3 activators, ALG2 was recruited to the plasma membrane pre-speck. This occurred through an unknown mechanism implied not to be GSDMD pores. The NLRP3 triggers Imiquimod, nigericin, ATP, LLOMe and crystalline matter were tested, and *Mtb* infection was not a part of the work.

Chapter 2

Theory

This chapter will present relevant research and theoretical background for the work presented within this thesis. First, the concept of cell cultivation and various related topics are introduced, as this forms the foundation for the employed model system. Thereafter, a section on *Mtb* and its molecular mechanisms of infection follows. Cellular mechanisms of interest in this work are thereafter presented: The NLRP3 inflammasome and its activation, followed by the ESCRT system, and the process of autophagy. Finally, fluorescence microscopy is explained, with a subsection containing details on TIRF microscopy, the most central technique employed in this project.

2.1 Cell cultivation

Providing a satisfactory environment is essential when studying cells outside of an organism. To ensure such conditions, cells are typically kept in a liquid called a *culture medium*, which supports cell proliferation. This medium contains salts, amino acids, glucose, fatty acids and vitamins, yielding a suitable ionic strength and access to nutrients. Furthermore, glutamine is present as a nitrogen source, and serum is added, as it contains proteins that support proliferation further. Antibiotics is commonly added to the culture medium in order avoid contamination. Cells in medium, referred to as *cultures*, are usually kept in vented flasks with hydrophilic coatings, and placed in incubators that ensures a suitable temperature, atmosphere and humidity. [9]

An important property of cells in culture is whether they are *adherent* or not. *Suspension cells* grow without attaching to a solid surface, as they are derived from blood, while adherent cells need to anchor to proliferate. Proliferation is thus limited by either the culture flask volume, or its surface area, as well as nutrient availability. To ensure that the cells thrive, it is therefore necessary to regularly supply a subpopulation of the cell suspension with fresh medium, and discard the remaining cells. Toxic metabolites are thereby removed, and fresh nutrients are provided. Additionally, the density of cells are kept in a range suitable for proliferation. This process is known as *splitting* the cells. The optimal frequency of splitting varies between cell lines and their growth rates, but is usually in the range of once every few days. [10]

2.1.1 Primary cells, secondary cells and cell lines

Cells in culture can be obtained from several different sources: *Primary* cell cultures consist of cells acquired directly from an animal or a plant, while *secondary* cell cultures are established with cells from a primary cell culture. Considerable genotypic uniformity can be obtained in a secondary cell culture, as there is only one type of donor cell. Such a cell population is termed a *cell line*. A cell line can also be made by cloning a single cell. [10]

Primary cells and cell lines are different in several ways. Primary cells can only divide a finite number of times before they die and thus have a shorter life span than cell lines. In contrast, cell lines are usually derived from cancer cells, providing them with an immortal nature. Such cells are therefore able to divide indefinitely and stay alive forever, if exposed to the right environment. Furthermore, primary cells are often more diverse than cells from a cell line, despite separation and sorting. The uniformity and continuity makes cell lines more suitable for experiments and genetic manipulation than primary cells. However, an important property of primary cells is their potentially greater resemblance to an *in vivo* situation. In a clinical setting, primary cell experiments are therefore often considered to be of higher relevance. [11]

2.1.2 Genetic manipulation

Cell lines can be altered in several ways in order to examine cellular processes. For instance, one can introduce new genes that encode fluorescently tagged versions of relevant proteins. This can be achieved though **viral transduction**: By bacterial cloning, *retroviruses* that encode the desired proteins are made. Such retroviruses use RNA as a template for DNA synthesis, and are used to infect cells. The viral DNA is thereafter integrated into the host genome, and thus transcribed. This way, the altered proteins are expressed, and their genetic encoding is transferred to daughter cells. [12]

Furthermore, another important manipulation mechanism is the bacterial **CRISPR-Cas9** system. *Clustered regularly interspaced short palindromic repeats* (CRIPSR) constitute a type of immune system in bacteria. Short DNA spacer sequences are induced as a response to viral infection, resulting in production of crDNA. Such crDNA give double-stranded breaks in foreign DNA by the use of *CRISPR-associated protein 9* (Cas9), protecting the bacteria. By introducing engineered CRISPR sequences that encode *guide-RNAs* into cells, together with Cas9 sequences, genomic DNA is cut at the locations specified by the guide-RNAs. Thus, the result is a knock-out of a gene of interest. This is commonly used to assess the role of various genes or to examine the effect of removing specific proteins. [13, 14]

2.2 *Mycobacterium tuberculosis* and the course of infection

Mycobacterium tuberculosis (Mtb) is the pathogen that causes tuberculosis, one of the top ten causes of death globally. In 2017 alone, 1.6 million people died from tuberculosis, and 10 million people developed the disease. [1]

The bacterium spreads between people through the air: When an infected individual sneezes or coughs, another person might breathe in droplets that contain *Mtb*. There are several possible outcomes after this: Clearance or resistance, latent infection, or active tuberculosis [15]. Subsequent to inhalation, alveolar macrophages recognize the bacteria and ingest them, described in more detail below. This eventually results in immunological signaling that drives recruitment of other types of immune cells, e.g. dendritic cells. They migrate to the lymph nodes to instruct the adaptive immune response after encountering the pathogen. As a consequence of activation of adaptive immunity, a *granuloma* forms around the bacteria. Such a granuloma consists of infected macrophages and other cells in the center, surrounded by an outer layer fibroblasts producing a fibrotic capsule, as well as B cells and T cells [16]. This state is considered the latent phase of tuberculosis. The granuloma represents a balance between the bacterium and the immune system; this phase of the disease can last for decades, and the infection is somewhat controlled. However, the bacterium can be reactivated and start replicating again, for instance

in cases where the immune system of the infected individual is weakened. This could result in spread of the bacteria to other tissues, and development of disease [17].

2.2.1 Molecular mechanisms of infection

Mtb, as other microbes, display pathogen-associated molecular patterns (PAMPs), which bind to and activate pathogen-recognition receptors (PRRs) at the plasma membrane of immune cells, in this case macrophages. This triggers phagocytosis of the bacterium. Subsequently, the phagosome that contains *Mtb* matures into a phagolysosome, as the cell tries to digest the microbe. [18]

Mtb has, however, evolved strategies to avoid degradation by the lysosomal enzymes. By inhibiting maturation of the phagosome, *Mtb* protects itself against digestion. Ultimately, the bacteria survive within the cell inside a compartment, protected from extracellular detection by antibodies, and from intracellular detection by receptors in the cytosol or on membranes. Autophagy, a cellular process described in section 2.5, has also been shown to target *Mtb* when permeabilization of the phagosome occurs. Microbial degradation via autophagy is termed *xenophagy*. [19]

By the use of early secretory antigenic target (ESAT-6) protein family secretion (ESX) systems, *Mtb* also manages to escape the phagosomal compartment and translocate into the cytosol [20]. This is thought to be achieved by ESAT-6 inserting into the membrane of the phagosome, forming a pore [3]. Such phagosomal escape can be detected with fluorescence microscopy by labeling *galectin 3* (gal3), a protein that binds carbohydrates usually positioned on the outside of the plasma membrane – or the inside of phagosomes [21, 22]. Once in the cytosol, the bacterium can replicate. Also, cytosolic PRRs gain access to the bacterium, for instance NLRP3, described in section 2.3. Such a recognition leads to inflammasome formation, inflammatory signaling, and eventually cell death.

2.3 The NLRP3 inflammasome

This section is based upon *Janeway's Immunobiology* by Kenneth Murphy and Casey Weaver [18], unless otherwise stated.

As mentioned above, a large complex termed an *inflammasome* can be receptor-activated by pathogens in the cytosol. Such inflammasomes form signaling platforms that are important players in inflammation. Their main role is to regulate maturation of the inflammatory cytokine *interleukin 1β* (IL-1β), allowing its extracellular release and subsequent binding to receptors.

Inflammasomes are large multiprotein complexes, and their assembly starts with activation of receptors, e.g. nucleotide oligomerization domain (NOD)-like receptors (NLRs). NLRs have a tripartite structure consisting of a C-terminal leucine-rich repeat domain, a central NOD, and an N-terminal protein-protein interaction domain, e.g. pyrin.

There are 14 different pyrin-domain NLR proteins in humans, and out of these, NLRP3 is the most widely studied. However, there is no known chemical link between the various ligands that result in NLRP3 activation. The exact molecular mechanism of its activation thus remains unclear, as is described in more detail below. Nevertheless, it is established that species that trigger a K^+ efflux often result in NLRP3 activation.

Upon activation, NLRP3 aggregation results in interaction between the pyrin domains of NLRP3 itself and the pyrin domains of *apoptosis-associated speck-like protein containing a caspase activation and recruitment domain (CARD)* (ASC). In the case of potassium-dependent NLRP3 activation, this could be mediated by the kinase NEK7 [23, 24]. In the ASC molecule, both the pyrin domain at the N-terminal and the CARD at the C-terminal can form polymeric filamentous structures. Because pro-caspase-1 also has a CARD, ASC can translate the NLRP3 aggregation into accumulation of this pro-enzyme. Such an assembly, illustrated in figure 2.1, is thought to drive the autocleavage of pro-caspase-1, resulting in activated caspase-1. Caspase-1 then processes pro-IL-1β and pro-IL-18 into their active forms.

As the ASC aggregate grows, it can eventually be observed by microscopy and is termed a *speck*. To observe such a speck, cells are commonly genetically manipulated to express ASC with a fluorescent tag, or immunolabeling is used. Normally, one speck forms per cell, and the observation of an ASC speck is thus used as a confirmation of inflammasome activation. [25]

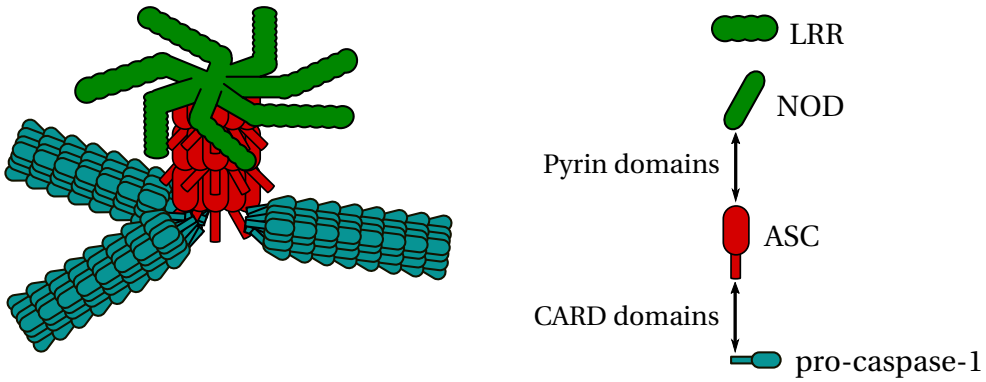

Figure 2.1: Illustration of the NLRP3 inflammasome architecture. The left side demonstrates the entirety of the complex, while the right side of the figure presents the molecules that compose the various parts, and their interaction.

2.3.1 Activation of the NLRP3 inflammasome

The leucine-rich repeat domain of the NLRs is thought to be bound by inhibiting chaperone proteins, keeping NLRP3 in an inactive form. This conformation of the inflammasome is thought to be located in endoplasmic reticulum structures [26]. In going from this state to an active form of NLRP3, there are two steps: *priming* and *activation*.

Priming is achieved by signaling through Toll-like receptors (TLRs) after binding of pathogen- or damage-associated molecular patterns (PAMPs or DAMPs), or through receptor-binding of tumor necrosis factor α (TNF-α) or other pro-inflammatory cytokines. This results in activation of the transcription factor NF-κB, giving increased levels of inactive NLRP3 and immature cytokines.

The activation can thereafter be achieved through multiple events: Reduction of intracellular potassium concentration, generation of reactive oxygen species (ROS), and destabilization of lysosomes. The latter is a route induced by particulate or crystalline species. As mentioned above, the exact activation mechanism of NLRP3 is disputed. It has been shown that mitochondria can be damaged as a part of the activation process, and it was recently suggested that oxidized mitochondrial DNA could be a point of convergence for all NLRP3 activating pathways [27]. Also, a 2018 study found that the *trans*-Golgi network disassembles post-stimuli and subsequently recruits NLRP3 through ionic bonding [28]. The authors suggest that this process promotes ASC oligomerization, thus acting as a shared NLRP3 activation route for various stimuli.

The importance of calcium and potassium ion fluxes in this context has also been discussed. Several reports have claimed that calcium-mediated damage of the mitochondria [29, 30, 31] or calcium-mediated support for ASC oligomerization through the TAK1-Jnk pathway [32, 33] are

driving forces behind NLRP3 inflammasome activation. However, calcium fluxes are a side effect of most potassium efflux-dependent inflammasome triggers, and has been shown to be dispensable for the NLRP3 activation [34]. This is further supported by how many of the studies on this topic are based on the calcium channel inhibitor 2-aminoethoxy diphenylborinate (2-APB), which also blocks NLRP3 activation, discrediting previous findings related to calcium dependency [35]. Thus, there is agreement that induction of potassium efflux is a feature of most NLRP3 triggers, while the necessity of calcium fluxes is disputed.

Following NLRP3 activation, cells often die through pyroptosis. This is an inflammatory form of cell death that starts by caspase-mediated cleavage of gasdermin D (GSDMD), a pore-forming protein. The N-terminal fragments oligomerize and form a plasma membrane pore. This pore allows release of IL-1β, but also ions fluxes in both directions, and influx of water. Eventually, this leads to swelling and lysis, with release of intracellular contents. [36, 37]

2.4 ESCRT and its role in plasma membrane repair

Upon damage to the plasma membrane, there are multiple possible routes of repair, two of which are illustrated in figure 2.2. One of the proposed mechanisms, shown in figure 2.2 A), is that Ca^{2+} enters the cell when permeabilization occurs, which induces lysosomal exocytosis, indicated by A1 in the figure. The lysosomal enzyme acid sphingomyelinase is thereby released, resulting in membrane remodeling and finally endocytosis of the wounds, indicated by A2 and A3 in the figure, respectively. [38]

In recent years, a plasma membrane repair pathway involving the endosomal sorting complex required for transport (ESCRT) has also been uncovered, illustrated in figure 2.2 B). Here, it is suggested that the Ca^{2+} influx through damaged areas recruits ESCRT proteins to the plasma membrane, as indicated by B1 in the figure. This results in budding vesicles, and the damaged parts of the membrane are pinched off and shedded, indicated by B2 and B3 in the figure, respectively. [39]

The role of ESCRT as a plasma membrane repair pathway was elucidated by a study from Jimenez *et al.* published in 2014. The authors damaged the plasma membrane in various ways, e.g. with micropipettes, detergents, pore-forming toxins and lasers [7]. Subsequently, ESCRT effects were studied. By examining propidium iodide (PI) fluorescence and entry kinetics, the group established size and closure rate of the plasma membrane wounds. Fluorescently labeled ESCRT proteins were observed to redistribute from the cytosol into localized, bright spots on the cell membrane, suggesting recruitment to positions of damage. By further analysis, it was found that ESCRT was essential particularly for repair of wounds smaller than 100 nm in diameter. It was excluded that lysosomes transport ESCRT proteins to the plasma membrane, disputing a

link between the above-mentioned systems. Energy-depleted cells and cells with impaired microtubules also displayed ESCRT recruitment to plasma membrane wounds, suggesting that the process is independent of vesicular transport. Further evidence was also found with correlative light electron microscopy (CLEM), showing colocalization of ESCRT proteins and clusters of extracellular buds.

Furthermore, another 2014 study, by Scheffer *et al.*, examined the effect of Ca^{2+} influx on recruitment of ESCRT proteins to the plasma membrane [40]. The ESCRT subunits consist of five complexes, which are recruited sequentially: ESCRT-0, ESCRT-I, ESCRT-II, ESCRT-III and ESCRT disassembly subcomplex. Scheffer *et al.* found membrane punctae containing the calcium-binding accessory protein apoptosis-linked gene 2 (ALG2) and an ESCRT-III protein both after inducing a large injury and after inducing an ionophore calcium flux. Removal of extracellular Ca^{2+} resulted in inhibition of this effect, and knockout studies showed that the ESCRT-III assembly at the wound site most likely is initiated by ALG2 and mediated by ALG2 interacting protein X (ALIX).

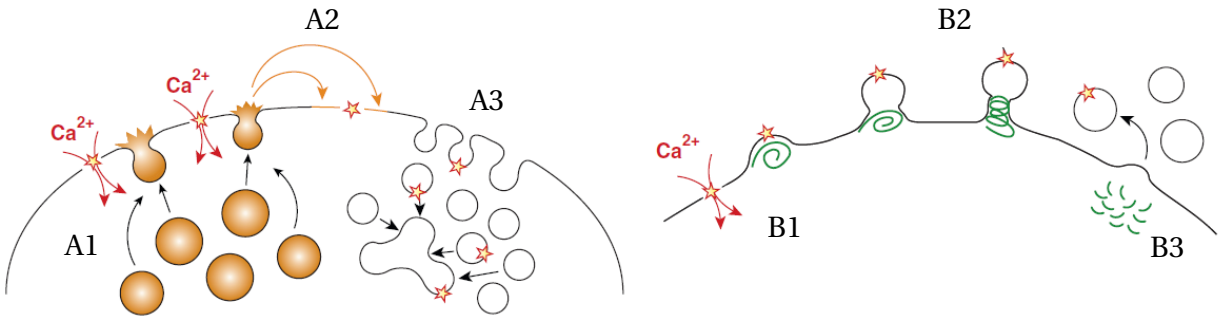

A) Lysosome-mediated plasma membrane repair

B) ESCRT-mediated plasma membrane repair

Figure 2.2: Illustration of the distinction between the proposed lysosomal route of plasma membrane repair, shown in **A)**, and the ESCRT-mediated plasma membrane repair, shown in **B)**. In **A)**, it is shown that Ca^{2+} enters the cell upon damage, which induces lysosomal exocytosis, indicated by A1. This leads to release of acid sphingomyelinase, which subsequently remodels the plasma membrane, as indicated by A2. Finally, wounds are endocytosed, indicated by A3. **B)** shows how ESCRT proteins are recruited to the plasma membrane after a Ca^{2+} influx through wounds, indicated by B1. Thereafter, the ESCRT proteins form budding vesicles, as indicated by B2. Finally, these vesicles are pinched off the cell, as indicated by B3. Adapted and reprinted from [39] with permission from Elsevier.

2.5 Autophagy

When a cellular structure is damaged or no longer needed, a process known as *autophagy* secures its degradation and recycling. This task is implemented through formation of a vacuole that merges with late endosomes or lysosomes, which contain digestive enzymes. There are two main types of autophagy: *Macrophagy*, where the feature to be degraded is wrapped in a double membrane from the ER; and *microphagy*, where smaller autophagic vacuoles bounded by a single phospholipid bilayer are made. The former process degrades organelles and other large structures, while the latter results in small cytoplasm-containing vesicles. Autophagy also functions as an energy-providing process during cellular starvation. [41]

2.5.1 Molecular players

Unc-51-like kinase 1 (ULK1) is a central autophagic protein. Initiation of autophagy is thought to happen through the nutrient-sensing kinase *mammalian target of rapamycin* (mTOR), which has inhibiting effects on ULK1 when nutrient levels are high, and the energy-sensing *AMP-activated protein kinase* (AMPK), which deactivates mTOR and activates ULK1 when energy is low [42]. When the cellular environment results in ULK1 activation, the kinase functions together with other proteins in an initiation complex. This complex is responsible for formation of the phagophore, which is the precursor for the autophagic membrane [43]. Furthermore, autophagy-related (ATG) genes encode *ATG factors*, a collective term for proteins that aid in the autophagic process [44]. They organize sub-complexes that eventually ligates phosphatidylethanolamine to *microtubule-associated proteins 1A/1B light chain 3* (LC3), enabling autophagic membrane growth [45, 46]. In relation to *Mtb*, LC3-labeled double membranes wrap around bacteria that have ruptured their phagosomal compartment, preparing it for degradation [47]. Exactly how the autophagy machinery targets the bacterium is not fully known, but cGAS-STING recognition of *Mtb* DNA resulting in ubiquitination has been shown, as well as a subsequent connection between ubiquitin and autophagy through Parkin and Smurf1 [48, 49, 50].

LC3-associated phagocytosis (LAP) is an additional function of LC3, besides autophagic membrane elongation. LAP shares some of the same molecular players with autophagy, but is independent of ULK1 and does not seem to be affected by cellular starvation or stress. The process is thought to be activated in parallel with phagocytosis, and LC3 is recruited to the phagosome by binding to various entities through an unknown mechanism. The LAP pathway is important for antigen presentation, degradation of extracellular species, and possibly also for utilizing nutrition from phagocytosed material [51]. Differentiation between xenophagy and LAP can be difficult if based only on an fluorescent LC3-tag [52]. However, LAP is suggested to occur prior

to phagosomal escape [53].

2.5.2 Secretory autophagy

In recent years, it has been discovered that autophagy also plays a role in a pathway termed *secretory autophagy*, a type of unconventional secretion which is independent of the established secretion mechanism through the ER and Golgi, as illustrated in figure 2.3. This unconventional pathway enables the cell to deliver molecules directly from the cytosol to the extracellular environment, with the help of autophagic machinery. Release of the cargo into the extracellular environment is achieved via SNARE proteins and plasma membrane syntaxins [54]. This pathway allows secretion of proteins that have extracellular functions but lack signaling peptides, proteins that form unwanted aggregates in the cytosol, partially degraded organelles, and bacteria. In the latter case, it is thought that secretory autophagy is a mechanism through which bacteria can spread from an infected cell to an uninfected one [55]. It is not fully established how the cell separates between substances for secretive versus conventional, degradative autophagy [56]. However, ESCRT-related proteins has been implicated in yeast and could be associated with the sorting [57].

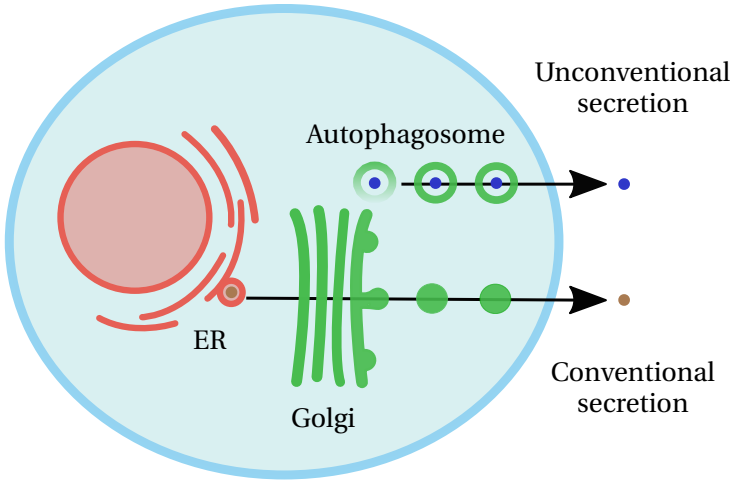

Figure 2.3: Illustration of the distinction between conventional secretion and secretory autophagy. Here, the lower route display conventional secretion of proteins through the ER and Golgi. The upper route illustrate the unconventional route of secretion through encapsulation in an autophagosome.

2.6 Fluorescence and fluorescence microscopy

This section will introduce the fundamental theory behind fluorescence microscopy. The contents herein are based upon theory from *Introduction to Biophotonics* by Paras N. Prasad [58], in addition to other sources that will be cited.

2.6.1 Fluorescence

Fluorescence is a quantum mechanical process where a molecule is de-excited from a high energy state into a lower energy state, and a photon with energy corresponding to their difference is released.

Typically, a molecule enters a high-energy state upon absorbing energy, for instance via the absorption of photons. Figure 2.4 a) shows a Jablonski diagram, which illustrates this process: The molecule starts out in a ground state, termed S_0, absorbs a photon with a certain energy, and ends up at a higher-energy state. From the excited state, several routes back to lower energy states are possible. An important de-excitation mechanism is vibrational relaxation, i.e., molecular heat releases, termed *non-radiative transition*. Here, the molecule is relaxed into a local energy minimum, referred to as S_1 in the diagram, through a series of smaller vibrational energy levels. The molecule can then transition into the ground state of a lower electronic state, achieved by the release of a photon. This is the process of fluorescence. The emitted photon thus have an energy corresponding to the difference between the two energy minima. The energy that is emitted in the form of a photon is therefore smaller than the energy that was originally absorbed. This is reflected in how the fluorescence emission energy spans a smaller range than the excitation energy in figure 2.4 a). All in all, this means that the excitation photons have shorter wavelength, i.e. larger energy, than the emission photons.

In practice, this concept is utilized in the technique of fluorescence microscopy, where a sample containing fluorescent molecules or dyes is excited with a specific wavelength of light. Resulting fluorescence emission from the sample, having a longer wavelength than the excitation light, is then collected and observed. Filters and dichroic mirrors (beamsplitters) ensure that the excitation light is allowed onto the sample, and that emission light reaches the detector without much background from other fluorescent sources, autofluorescence or excitation light. Thus, one aims at achieving the regime where only the fluorescent molecules are observed.

The excitation light source in a fluorescence microscope has to be intense, and close to monochromatic. Lasers possess both these properties and are therefore commonly used, especially for complex techniques such as total internal reflection fluorescence (TIRF) and confocal microscopy [59]. For any given fluorescent molecule, a range of wavelengths give excitation at various efficacies. One needs a sufficient amount of fluorescing molecules to achieve a strong

signal, and therefore, as much as possible of the incoming light should be absorbed. An *excitation spectrum* shows the absorption versus the wavelength of the excitation light for a specific fluorescent compound. Such a plot advises the reader on which wavelengths yield the highest absorption, i.e., which laser is optimal to use for excitation of the molecule. Furthermore, the *emission spectrum* shows the wavelengths that are emitted from a specific fluorescent compound, and at what intensities. These features are illustrated in figure 2.4 b). The *Stokes shift* denotes the distance between the peaks in the two spectra, and its size is related to the relaxation process that occurs in the molecule between excitation and emission. The Stokes shift has to be sufficiently large so that excitation and emission can be separated by the available filters in a microscope.

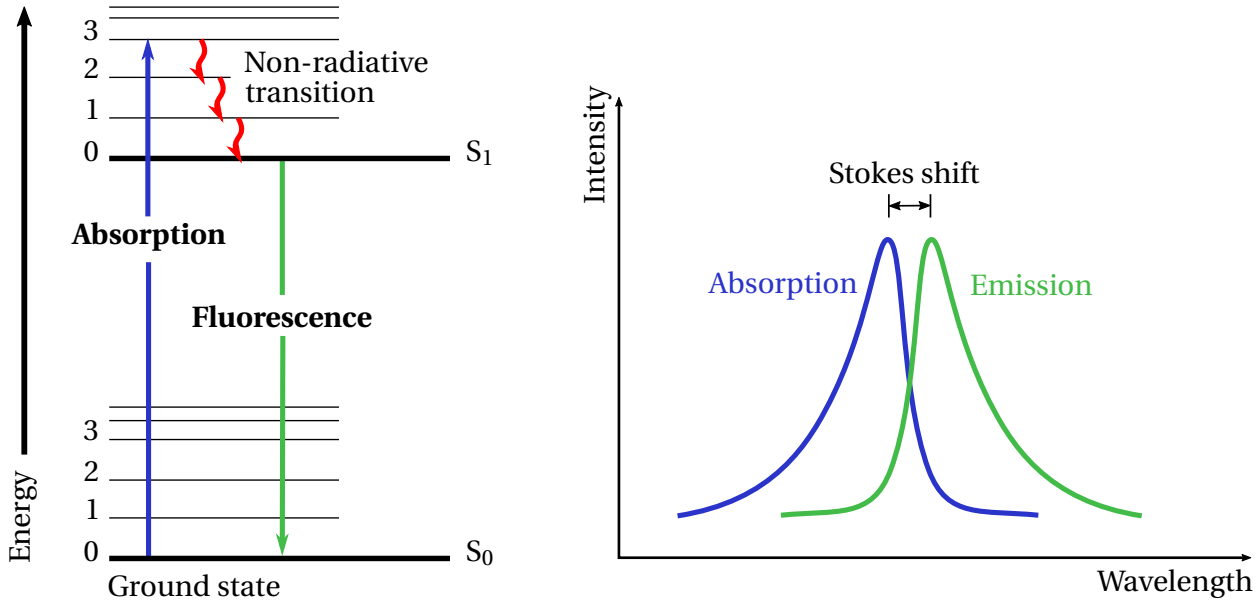

(a) Jablonski diagram

(b) Stokes shift

Figure 2.4: This figure illustrates two central concepts behind fluorescence: **(a)** shows a Jablonski diagram, which demonstrates the electronic transitions that can result in fluorescence. **(b)** shows an illustration of typical absorption and emission spectra, where the wavelengths that are most absorbed and emitted as fluorescence for a specific compound can be seen. The energy difference between the peak absorption and peak emission is called the Stokes shift.

Fluorescent markers

In order to observe cellular features with fluorescence microscopy, they are usually bound to a fluorescent molecule. To achieve this, one approach is to add fluorescent dyes that bind specifically to a certain type of structure or a certain compound. Another approach is to genetically manipulate the cells' genome so that fluorescent versions of proteins of interest are expressed,

as outlined in section 2.1.2. This is accomplished by fusing the relevant features to fluorescent proteins, such as the well-known Green Fluorescent Protein (GFP). A paper describing how to fuse GFP to any protein of interest was published in 1994 [60], and since then, countless fluorescent proteins have been discovered, improved and developed. This has revolutionized the field by enabling observation of behavior and interactions of cellular features, providing endless amounts of new knowledge [61].

2.6.2 Live-cell imaging

While imaging live cells, the impact of external factors that affect the cellular functions must be minimized. Therefore, several challenges must be met. As cells need physiological temperature and a satisfactory atmosphere and humidity, incubators are often installed around the sample stage on live-cell imaging platforms. Furthermore, to avoid phototoxicity, extra care should be taken to avoid high laser intensities and damaging wavelengths when imaging live cells. Fluorescent marker overexpression could also be a source of cytotoxicity, as well as toxic effect from dyes. [62]

In TIRF microscopy, described in more detail below, only a small section of the cell is illuminated. The lower overall laser exposure limits phototoxicity effects as compared to widefield and confocal microscopy. This makes the TIRF microscopy technique an advantageous option for live-cell imaging. Furthermore, the technique offers low background and high signal-to-noise ratio, because negligible fluorophore excitation occurs in the rest of the cell, i.e. outside of the illuminated section.

2.6.3 Total Internal Reflection Fluorescence Microscopy

TIRF microscopy is a technique where imaging of a small zone near the coverslip, typically ~100 nm deep, is made possible. This is achieved by utilizing a phenomena that occurs when light hits an interface between two media: As light propagates through a medium with a refractive index of n_1, e.g. glass, and encounters the interface to a medium with a lower refractive index n_2, e.g. cell medium, it is reflected if the refractive angle is large enough. This event, illustrated in figure 2.5, is known as *total internal reflection* (TIR). Such reflection occurs when the angle of incidence is larger than a certain critical angle, θ_c. Using Snell's law, θ_c can be derived as follows [63]:

$$n_1 \cdot \sin\theta_1 = n_2 \cdot \sin\theta_2 \Rightarrow \sin\theta_c = \frac{n_2}{n_1} \cdot \sin(90°) \Rightarrow \theta_c = \sin^{-1}\frac{n_2}{n_1} \tag{2.1}$$

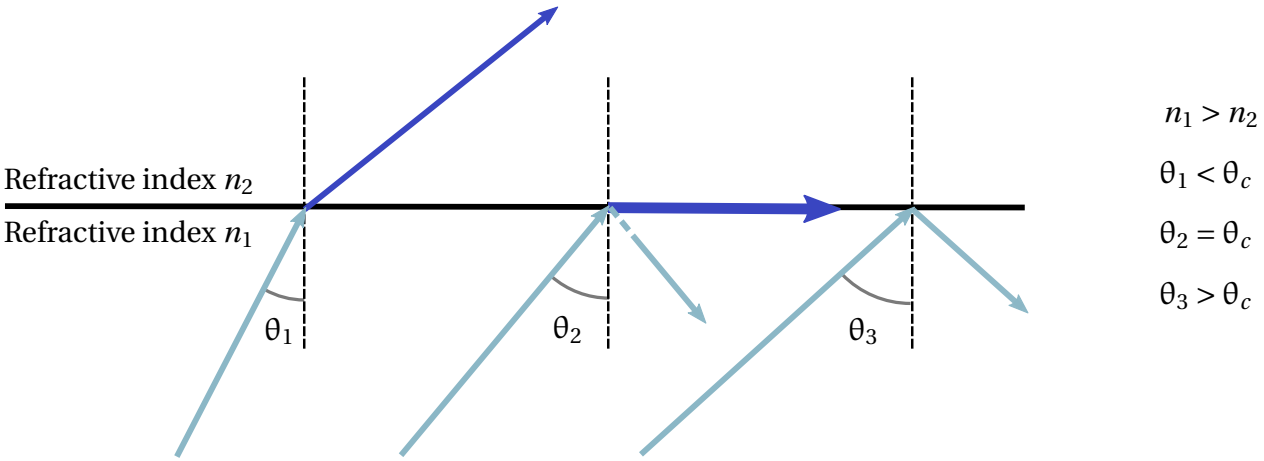

Figure 2.5: This figure shows the principle upon which TIRF microscopy is based. θ_c denotes the critical angle: Light incoming at the interface at an higher angle than this will be totally internally reflected.

Evidently, an angle of incidence larger than θ_c results in total internal reflection of the incoming light, if the refractive indices n fulfil the requirements mentioned above.

Glass has a refractive index of 1.52, while cells usually reside in aqueous buffers with a refractive index of 1.33 [64]. For a system where cells in an aqueous medium rest on a glass substrate, the critical angle for TIR should thus be:

$$\theta_c = \sin^{-1}\frac{1.33}{1.52} \approx 61° \tag{2.2}$$

Incoming light that hits the glass-cell interface at an equal or higher angle is thus totally internally reflected, given that the numerical aperture of the employed objective is large enough.

When TIR is achieved, a small portion of the incoming light still penetrates the interface. This energy is known as the *evanescent wave*, characterized by rapidly decaying intensity (i.e., electric field amplitude), which enables the very narrow excitation utilized for TIRF microscopy [65]. This wave excites only the fluorescent molecules in the ~100 nm of cellular environment that is closest to the glass interface. Cells to be observed with TIRF microscopy therefore have to be adherent, as suspension cells are too far away from the interface to be seen.

The typical setup of a TIRF microscope is shown in figure 2.6. Laser illumination exits the objective at an angle larger than the critical angle and eventually hits the glass-cell interface. Here, the beam is totally internally reflected, and the evanescent wave gives excitation of a thin zone in the cellular environment. Resulting fluorescence emission is collected, and the user is able to observe the cell membrane, excluding most of the signal from the cytoplasm.

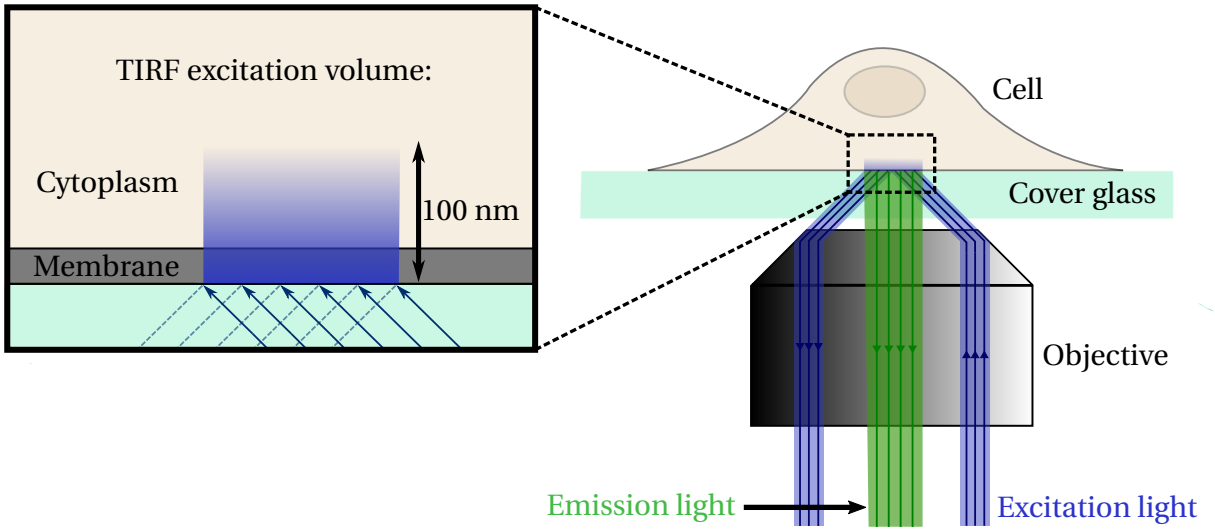

Figure 2.6: Illustration of how a TIRF microscope functions. Light exits the objective at an angle equal to or larger than the critical angle, as shown with the blue lines, and is reflected at the interface between the glass and the cellular environment. Here, an evanescent wave excites fluorophores in a small volume close to the glass coverslip, as illustrated in the zoom-in. Fluorescence emission light from this small volume, shown as green lines, is thereafter collected.

Chapter 3

Materials and methods

This chapter will present the experimental procedures as they were carried out, and the cells, reagents and equipment that were used. First, the methods by which cells were cultured and prepared for experiments is described, followed by specific procedures for bacterial cell cultures. Thereafter, the NLRP3 stimuli and bacterial infection protocols are described, in addition to descriptions of how autophagy was inhibited and how calcium flux imaging was done. Fluorescence microscopy settings and procedures follows this. Finally, there is a section on interpretation and analysis of the results.

3.1 Cell cultivation and differentiation

In general, cells were cultured in Roswell Park Memorial Institute (RPMI) 1640 medium (*Sigma*) in T-25 Corning cell culture flasks (*Sigma*). The medium was supplemented with 10% fetal calf serum (FCS) (*Gibco*), 1% penicillin streptomycin (P/S) (*Gibco*), 3.4% L-glutamine (*Gibco*), and 1% 4-(2-hydroxyethyl)-1-piperazineethanesulfonic acid (HEPES)-Triton buffer 1 M (*Gibco*). Hereafter, RPMI with all supplements will be referred to as *complete RPMI*. The cultures were kept inside an incubator cabinet (*Thermo Scientific*) that ensured a temperature of 37 °C and an atmosphere containing 5% CO_2.

The monocytic suspension cell line THP-1 [66] was utilized in all experiments. Viral transduction was used to introduce constitutive expression of fluorescent variants of relevant proteins, and several cell lines with different combinations of fluorescent proteins of interest were made. Proteins were fused to either mNeonGreen (excitation maximum 506 nm, emission maximum 517 nm) [67], mScarlet (excitation maximum 569 nm, emission maximum 594 nm) [68], mIRFP670 (excitation maximum 690 nm, emission maximum 713 nm) [69], or SNAP [70]. This work was performed by Kai Sandvold Beckwith and will not be elaborated upon in this thesis. The cell lines and the fluorescently tagged proteins they contain are presented in table 3.1. These will hereafter be referred to by their abbreviation.

Abbreviation	**Fluorescent proteins**		
AGA	ALG2-mNG	Gal3-mSc	ASC-mIRFP670
AA	ALG2-mNG		ASC-mIRFP670
AGL	ALG2-mNG	Gal3-mSc	LC3-SNAP
AG	ALG2-mNG		Gal3-SNAP

Table 3.1: This table presents an overview of the cell lines used in the work. Abbreviations for each cell line are shown in the left column, and the fluorescent proteins the cell lines contain are shown in the right column.

In cell lines with SNAP-tagged proteins, the dye SNAPCell 647-SiR (*New England Biolabs*, excitation maximum 645 nm, emission maximum 661 nm) in complete RPMI was added to the cells at a concentration of 1.5 µM and incubated for 20-30 minutes. Thereafter, the cells were washed three times with complete RPMI, and incubated for an additional 20-30 minutes before experiments.

Cells were routinely counted by the use of EVE cell counting slides (*NanoEnTek*) and a Countess automated cell counter (*Invitrogen*). By splitting the cultures regularly, the cell concentration was kept between 200 000 and 1 000 000 cells per ml.

In preparation for experiments, cells were split to approximately 300 000 cells/ml, and phorbol 12-myristate 13-acetate (PMA) was added to the suspension to a final concentration of 100 ng/ml. This promotes differentiation of the monocytic cells into an adherent, macrophage-like phenotype. Thereafter, 100 µl was seeded out in each well in a 96-well glass-bottom plate with polystyrene frame (*Cellvis*, P96-1.5H-N, #1.5 high performance cover glass (0.170 ± 0.005mm)), resulting in an approximate concentration of 30 000 cells per well. After three days, the medium in the wells was changed to complete RPMI. Experiments were conducted within the subsequent three days.

3.1.1 Bacteria culture

The leucine and pantothenate auxotroph *Mtb* $mc^2$6206 [71] was cultured in Middlebrook 7H9 Broth (*BD Biosciences*) adjusted with 10% OADC, 0.05% Tween-80, 24 µg/ml D-pantothenate, and 50 µg/ml L-leucine. During growth, 10 ml culture was kept in 50 ml screw cap tubes (*Sarstedt*) in a shaking incubator (*New Brunswick Scientific*, Excella E24). The cultures were split regularly to keep the optical density (OD) in the log phase range. Glycerol was added to the new culture to a final level of 0.2% when splitting. The cultures were used for experiments for no more than 3 weeks after inoculation from freeze stock.

3.2 NLRP3 stimuli and *Mtb* mc^{2}6206 infection

In order to study the molecular mechanisms of infection, cells were incubated with *Mtb* mc^{2}6206. For comparison, cells were also stimulated with nanosilica, an NLRP3 activator that disrupt lysosomal function. The procedures are described below.

3.2.1 Nano-SiO_2 treatment

Nano-SiO_2 (*Invivogen*), hereafter referred to as nanosilica, was suspended in complete RPMI to a final concentration of 200 µg/ml. The regular medium in the wells was taken out, and 100 µl of the nanosilica suspension was added. In some cases, the cells were primed with 10 ng/ml LPS for 1-4 hours to ensure a quicker response.

3.2.2 *Mtb* mc^{2}6206 infection

When infecting cells with *Mtb* mc^{2}6206, the medium in the wells was exchanged for a bacteria suspension that was colored and prepared as follows.

The OD of the bacteria culture was measured using an Ultrospec 10 cell density meter (*Amersham Biosciences*) with 7H9 Broth as the blank. An OD between 0.45 and 0.6 was preferred. Approximately 4 ml of the culture was thereafter taken out and spun down in a Rotina 420R sentrifuge (*Hettich*) at 4754 RPM for 5 minutes.

The supernatant was discarded, and the pellet resuspended in 1 ml PBS with 0.05% Tween-80. The dye eFluor 450 (*eBioscience*, excitation maximum 405 nm, emission maximum 446 nm) was added to a final concentration of 5 µM, and the suspension was thereafter incubated for 15-30 minutes.

Following the incubation, the suspension was once again spun down at 4754 RPM for 5 minutes. The resulting supernatant was discarded, and the pellet was resuspended in 4 ml RPMI with 3.4% L-glutamine, 1% HEPES and 10% freshly thawed human serum (A+). The new suspension was then sonicated in an ultrasonic cleaner bath (*VWR*) at maximum power for 1 minute, and thoroughly vortexed.

Subsequently, the suspension was spun down at 300 RPM for 4 minutes to remove the largest aggregates. The OD was then measured again, with RPMI as the blank. The suspension was diluted to the desired infection OD, i.e. between 0.04 and 0.05.

Such a colored bacteria suspension was used for infection experiments within three days after preparation.

3.2.3 Inhibition and knockdown of autophagy

To study the effects of inhibiting autophagy, cells were treated with ULK1/2 inhibitor MRT68921 hydrochloride (*Sigma*) [72], hereafter referred to as MRT, during infection with *Mtb* mc^{2}6206. For approximately 1 hour pre-experiment, the cells were treated with either 2 µM or 5 µM MRT in complete RPMI. This concentration of the inhibitor was kept constant throughout the infection. The cells were infected with *Mtb* mc^{2}6206 by exchanging the medium in the wells for a colored bacteria suspension with an OD of 0.04-0.05, and imaged by TIRF and widefield fluorescence microscopy time-lapse imaging.

An ATG-5 knockdown AGL-cell line was also used for infection experiments. The knockdown was achieved through the CRISPR-Cas9 technique. This work was done by Kai Sandvold Beckwith and will not be elaborated upon in this thesis.

3.2.4 Calcium flux imaging with Calbryte

The calcium flux in the cells during NLRP3 stimuli and *Mtb* mc^{2}6206 infection was monitored by loading the cells with Calbryte 590 AM (*AAT Bioquest*, excitation maximum 580 nm, emission maximum 592 nm), hereafter referred to as Calbryte, a dye that binds weakly to calcium and becomes fluorescent when bound.

The Calbryte solution was prepared by adding the dye to Hanks buffer with 0.02% F-127 to a final concentration of 2 µM. To load the cells, the medium in the wells was replaced with 100 µl of this solution. The plate was subsequently incubated for 1 hour, and the medium was thereafter changed back to complete RPMI and incubated at room temperature for 15 minutes. Experiments were started within 6 hours after this.

Validation with ATP and saponin

The Calbryte system was tested with 3 mM ATP in complete RPMI, which induces a calcium influx through ion channels. Furthermore, the system was tested with 0.05% saponin in complete RPMI, which forms plasma membrane pores.

For both validation schemes, the medium in the wells containing Calbryte-loaded AA-cells was exchanged. Subsequently, the ALG2 effects at the plasma membrane and the changes in Calbryte intensity was examined with TIRF and widefield fluorescence microscopy time-lapse imaging.

Monitoring the calcium flux in cells that are treated with nanosilica

To examine how the calcium flux changes during treatment with nanosilica, AA-cells were loaded with Calbryte, and subsequently stimulated with 200 µg/ml nanosilica in complete RPMI by exchanging the medium in the wells for the nanosilica suspension. The Calbryte response and the events involving the tagged proteins were recorded with TIRF and widefield fluorescence microscopy time-lapse imaging.

Monitoring the calcium flux in cells that are infected with *Mtb* mc^{2}6206

To examine how the calcium flux changes during infection with *Mtb* mc^{2}6206, AA- and AG-cells were loaded with Calbryte, and subsequently infected with *Mtb* mc^{2}6206 by exchanging the medium in the wells for a colored bacteria suspension in RPMI, with OD 0.04-0.05. The Calbryte response and the events involving the tagged proteins were recorded with TIRF and widefield fluorescence microscopy time-lapse imaging.

3.2.5 Lysosomal damage control experiment

A control experiment where AGL-cells were loaded with the photosensitive chemical $TPCS_{2a}$ [77] was also performed. In a dark room, the medium in the wells were exchanged for a solution of 0.4 µg/ml $TPCS_{2a}$ (*PCI Biotech*) in complete RPMI, and the plate was incubated for 18 hours. Following this, the wells were washed three times with complete RPMI, and incubated for 4 hours before experiments.

To damage the lysosomes, i.e. activate the compound, the cells were illuminated with the 405 nm laser line at 10% power for 1 second. The subsequent events involving the tagged proteins were observed with TIRF microscopy.

3.3 Fluorescence microscopy

The cellular responses were studied with TIRF and widefield fluorescence microscopy. This section summarizes the settings that were used.

3.3.1 TIRF microscopy

The cells were observed before and during stimuli by the use of a ZEISS Laser TIRF 3 microscope. The microscope is enclosed by an incubator, which was set to 37 °C and 5% CO_2 approximately 30 minutes before experiments.

Most experiments were time-lapse imaging setups where a new frame was captured every 10 seconds. Furthermore, definite autofocus was enabled. One TIRF channel was chosen as the reference channel, and all the other TIRF channels had zero offset from this. All widefield channels had 2 µm offset from the reference, and the brightfield channel was offset with 5 µm. Table 3.2 displays the various laser lines and how they were employed to observe of the features of interest.

Laser wavelength	**Protein or dye**	**Laser intensity**	**Exposure**	**TIRF angle**
405 nm	eFluor 450	0.3%	200 ms	0°
488 nm	ALG2-mNG	0.2-0.3%	100 ms	0° and 71°
561 nm	Calbryte	0.2-0.3%	25-100 ms	0°
	Gal3-mSc	0.2%	25 ms	0° and 71°
638 nm	Gal3-SNAP	0.3%	100 ms	0° and 71°
	LC3B-SNAP	0.3%	100 ms	0° and 71°
	ASC-mIRFP670	0.6%	300 ms	0°

Table 3.2: This table shows an overview of the general microscope settings.

The filter cubes **76 HE CFP / GFP / DsRed** and **77 HE GFP / mRFP / Alexa633** were used in all experiments. Their relevant excitation and emission windows are presented in table 3.3. For brightfield imaging, a halogen lamp at 4.6 V with 0.91 ms exposure and a DIC-filter was used.

Filter name	Excitation windows	Emission windows
76 HE CFP / GFP / DsRed	390 nm – 422 nm	448 nm – 472 nm
	549 nm – 573 nm	585 nm – 631 nm
77 HE GFP / mRFP / Alexa633	469 nm – 497 nm	510 nm – 542 nm
	552 nm – 577 nm	587 nm – 614 nm
	629 nm – 650 nm	665 nm – 711 nm

Table 3.3: This table shows an overview of the filters that were used in the imaging setups, and their relevant excitation and emission windows.

3.4 Image analysis

In general, the ImageJ distribution FIJI [73] was used for image processing such as cropping, inserting scale bars and zoomed insets, adjusting of brightness and contrast, and changing lookup tables. Furthermore, the region of interest (ROI) manager in FIJI was used to analyze gray value changes at relevant sites, as described in the below subsections. The open-source vector graphics software Inkscape was used for creating figures.

Analysis of Calbryte imaging

For analyzing the Calbryte intensity changes during various cellular events, ROIs were chosen in image areas that were contained within the cell through the time period of interest, and had negligible crosstalk. The measurement tool was thereafter used to measure the mean gray value in the ROIs in the Calbryte channel through the whole image stack, i.e. at all the time points.

Analysis of LC3B imaging

The recruitment of LC3B to gal3-positive vesicles was analyzed by firstly drawing ROIs around compartments that turn gal3-positive while being LC3B-negative, ensuring that their movement throughout the time period of interest was included. Subsequently, the mean gray value of the LC3B-signal in the ROIs was measured through the whole image stack, i.e. at all the time points.

3.4.1 Plotting

In each experiment, frames with events of interest, i.e. the initiation of an ALG2 plasma membrane recruitment event or a phagosome turning gal3-positive, were identified. The mean gray value measurements in a specific range of frames before and after the event were located and saved, ensuring alignment of the measurements to the event of interest. Thereafter, all the data sets were normalized to the measurement obtained from the respective first frames of the chosen range. Ten individual events were used in all cases. Subsequently, the median and interquartile range of the normalized measurements were plotted using GraphPad Prism version 5.03 for Windows, GraphPad Software, La Jolla California USA, www.graphpad.com.

To decide if the results were significant, the Mann-Whitney U test was performed using an online calculator [74].

Chapter 4

Results

This chapter will describe the results from the investigation of various fluorescently tagged proteins during NLRP3 stimuli and *Mtb* mc^{2}6206 infection, outlined in Chapter 3. All results are based on images captured with TIRF and widefield microscopy.

Some general features of the cellular responses will be presented first, in order to introduce the reader to events of interest. This is followed by results regarding the interplay between gal3-positive phagosomes and ALG2 at the plasma membrane. Thereafter, results from imaging of autophagy protein LC3B during infection, and their analysis, are described. A summary of the effects seen on NLRP3 inflammasome activation during both nanosilica treatment and *Mtb* mc^{2}6206 infection follows. Finally, results from the calcium flux imaging and their analysis are presented. In the end of the chapter, there is a section showing control experiments.

4.1 Imaging of the events during *Mtb* mc^{2}6206 infection

Figure 4.1 displays a representative single AGA-cell that has been infected with *Mtb* mc^{2}6206 by exchanging the cell medium for a colored bacteria suspension with OD 0.04-0.05, and time-lapse imaged with TIRF and widefield fluorescence microscopy. Here, some of the events that occur during infection are shown: The top panel shows the gal3-mSc widefield signal. In the second frame, a compartment shows recruitment of gal3, as indicated by the inset. This suggests phagosomal escape and will hereafter be referred to as a *gal3-event* or the compartment becoming *gal3-positive*. The second panel shows the ALG2-mNG TIRF signal, and recruitment into a massive, bright spot is seen from the third frame, happening locally to the same position as the gal3-positive phagosome. Furthermore, there is a transient, more evenly distributed recruitment of ALG2 to the plasma membrane happening, as shown in the bottom inset in the fourth frame. The plasma membrane accumulation thereafter retracts, as seen in the last frame.

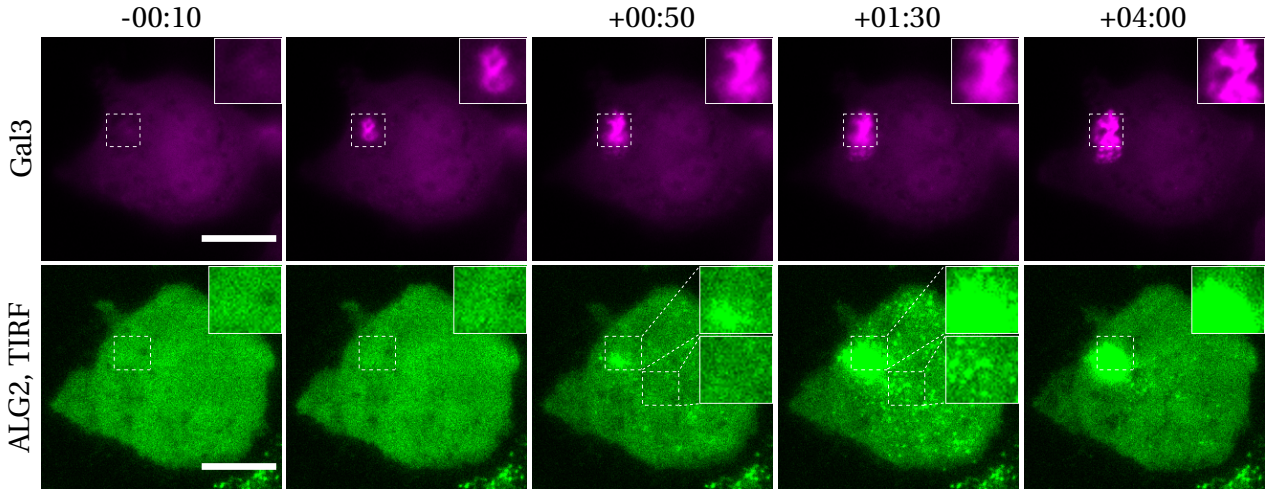

Figure 4.1: This figure shows some of the common events that occur in a single cell that is infected with *Mtb* mc^{2}6206. The top panel shows the gal3-mSc widefield signal, and the bottom panel shows the ALG2-mNG TIRF signal. Scale bars equal 20 µm, and the timepoints relative to the second frame are indicated above each column. Insets show 3x magnifications of the dashed areas. As can be seen from the insets, the gal3-mSc signal shows phagosomal escape in the second frame. Furthermore, a massive, local plasma membrane recruitment event happens in the same position, as seen in the ALG2-mNG TIRF signal in the next column. There is also a more evenly distributed and weaker recruitment of ALG2 into a starry pattern, as shown by the bottom insets in the ALG2-mNG panel, columns 3 and 4.

4.2 Gal3-positive phagosomes come close to the plasma membrane, triggering ALG2-recruitment

Recruitment of ALG2 to the plasma membrane during nanosilica NLRP3 stimuli and *Mtb* $mc^2$6206 infection has unknown origin. It was discovered that quite often when an ALG2-event occurred at the plasma membrane, a gal3-positive phagosome was positioned in the same area, intracellularly. In some of these cases, the gal3-positive compartment becomes visible in the TIRF mode, suggesting that it is close to the plasma membrane. The results showing this will be presented in this section.

4.2.1 Gal3-positive compartments during nanosilica treatment

Figure 4.2 shows the representative development in a single cell that has been stimulated with 200 µg/ml nanosilica in complete RPMI by exchanging the medium in the wells. The top panel shows the gal3-mSc widefield signal, the middle panel shows the gal3-mSc TIRF signal, and the bottom panel shows the ALG2-mNG TIRF signal. The two bottom panels thus show signal from fluorescent proteins that are close to the plasma membrane. Time points relative to the second frame are indicated above each column, and the insets are 3x magnifications of the dashed areas. The scale bars equal 10 µm. As is shown in the images, a phagosome containing a large silica crystal turns gal3-positive at time zero. Then, after some time, this gal3-positive compartment gets close to the plasma membrane, becoming detectable in the TIRF channel. Following this, an ALG2-event happens at the same location.

There were a total of 107 cells expressing gal3-mSc (88 AGA-cells, 19 AGL-cells) that were studied during nanosilica treatment. 44 compartments became gal3-positive during observation (28 in AGA-cells, 16 in AGL-cells), and there was a total of 28 pre-speck ALG2 plasma membrane recruitment events (24 in AGA-cells, 4 in AGL-cells). 15 of these ALG2 plasma membrane recruitment events were large, local accumulations at sites of gal3-positive phagosomes (11 in AGA-cells, 4 in AGL-cells).

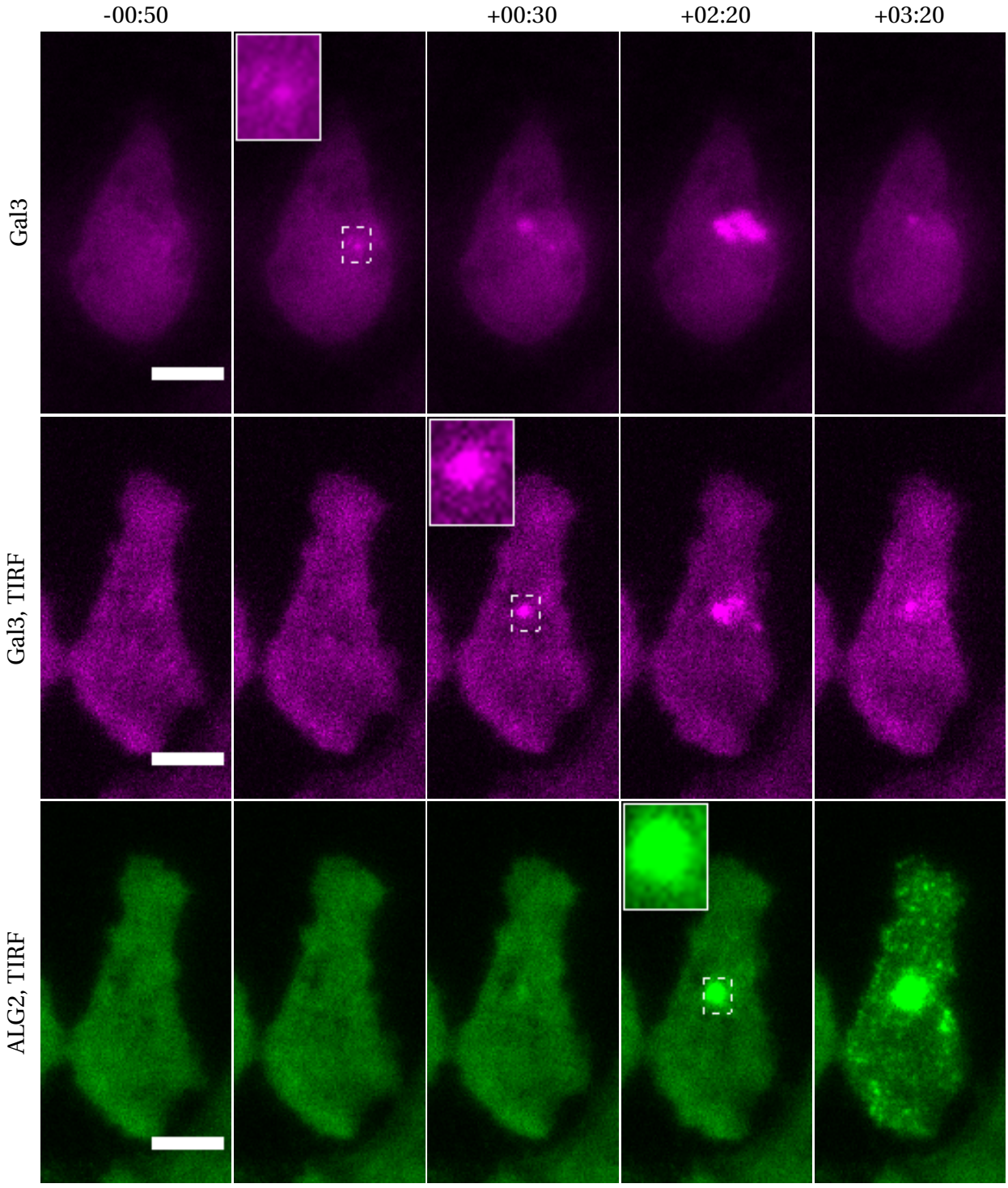

Figure 4.2: This figure shows a single cell that has been treated with nanosilica. The top panel shows the gal3-mSc widefield signal, the middle panel shows the gal3-mSc TIRF signal and the bottom panel shows the ALG2-mNG TIRF signal. The scale bars equal 10 µm, and the time points relative to the second frame are indicated in the top. Insets show 3x magnifications of the dashed areas.

4.2.2 Gal3-positive compartments during *Mtb* mc^{2}6206 infection

Figure 4.3 shows the representative development in a single cell that has been infected with *Mtb* mc^{2}6206 by exchanging the medium in the well for a colored bacteria suspension with an OD of 0.04-0.05. The top panel shows the gal3-mSc widefield signal, the middle panel shows the gal3-mSc TIRF signal, and the bottom panel shows the ALG2-mNG TIRF signal. The two bottom panels thus show signal from fluorescent proteins that are close to the plasma membrane. Time points relative to the second frame are indicated above each column, and the insets are 2x magnifications of the dashed areas. As is shown in the images, a phagosome containing a bacterium turns gal3-positive at time zero. Then, after some time, the gal3-positive compartment gets close to the plasma membrane, becoming detectable in the TIRF channel, as seen in the third frame in the second panel. Following this, an ALG2-event happens at the same location. By clicking or scanning the QR-code found in figure 4.4, the reader will follow a link to a movie of a cell that displays these features.

In total, there were 195 gal3-mSc-expressing cells that were time-lapse-imaged for 2 subsequent hours after infection with *Mtb* mc^{2}6206 (84 AGA-cells, 111 AGL-cells). In these, 100 mycobacterium-containing compartments became gal3-positive (59 in AGA-cells, 41 in AGL-cells), and there were 50 ALG2 plasma membrane recruitment events (25 in AGA-cells, 25 in AGL-cells). 28 of these ALG2-events were large, local accumulations at sites of gal3-positive compartments (18 in AGA-cells, 10 in AGL-cells).

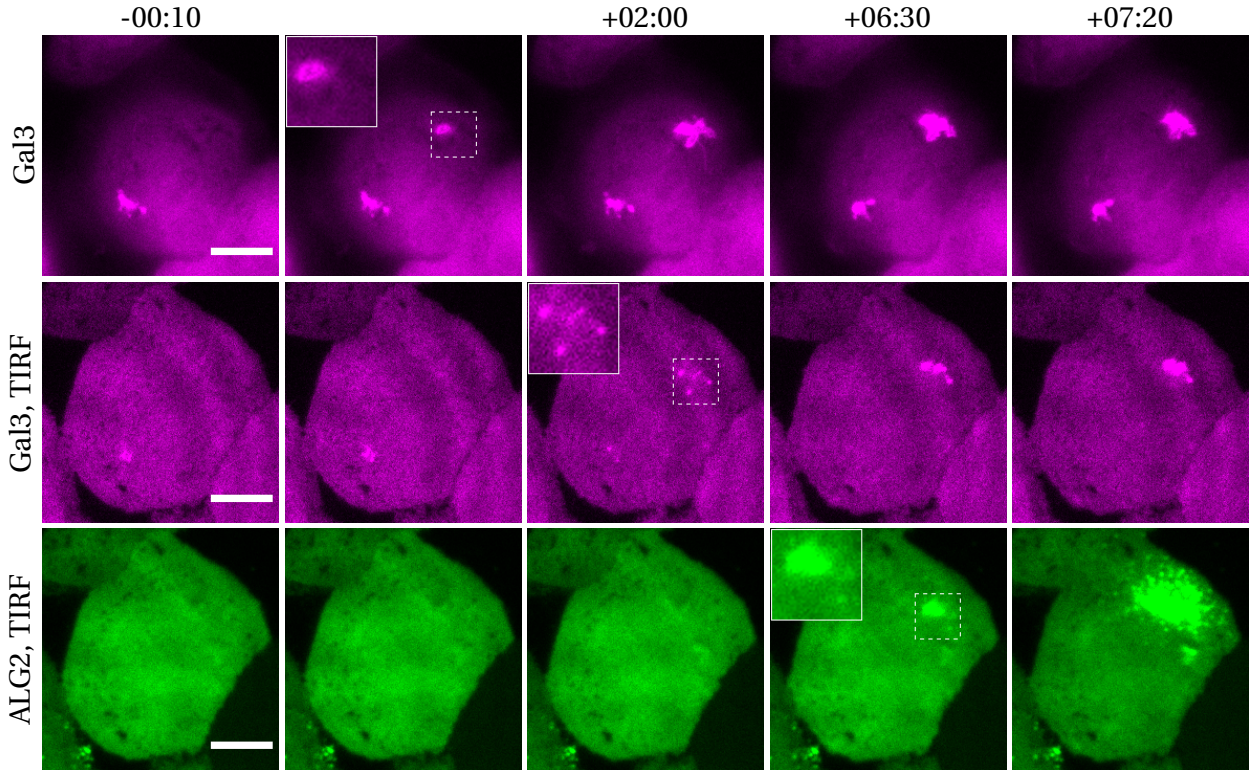

Figure 4.3: This figure shows a single cell that has been infected with *Mtb* mc^{2}6206. The top panel shows the gal3-mSc widefield signal, the middle panel shows the gal3-mSc TIRF signal and the bottom panel shows the ALG2-mNG TIRF signal. The scale bars equal 15 µm, and the time points relative to the second frame are indicated above each column. Insets show 2x magnifications of the dashed areas.

Figure 4.4: By scanning or clicking the above QR-code, the reader will gain access to a movie of events similar to those shown in figure 4.3. Here, the *Mtb* mc^{2}6206-containing compartment turning gal3-positive (left) and showing up in TIRF-mode (middle) occur in the same frame. A large ALG2 recruitment event is subsequently seen in the TIRF-mode (right).

4.3 Autophagy machinery is recruited to gal3-positive phagosomes

As mentioned in the theory section, autophagy proteins are known to be recruited to bacteria in the defense mechanism of xenophagy, and autophagic machinery has also been implicated in relation to ejection of bacteria. ALG2 could play a role here as well, as there could be a rupture of the plasma membrane during the course of the ejection. Therefore, autophagy-related protein LC3B fused to a SNAP-tag was investigated together with ALG2-mNG and gal3-mSc in order to examine the interplay between these proteins during *Mtb* mc^{2}6206 infection.

Imaging of AGL-cells during *Mtb* mc^{2}6206 infection

Cells were infected with *Mtb* mc^{2}6206 by exchanging the cell medium for a colored bacteria suspension in RPMI with an OD between 0.04 and 0.05. Subsequently, they were imaged with fluorescence microscopy time-lapse imaging for approximately 2 hours. Figure 4.5 shows a representative result. This single cell phagocytoses a bacterium, indicated by an arrow in the first frame. The bacterium escapes its compartment at time zero, indicated by the phagosome turning gal3-positive in the middle frame of the top panel. LC3B-SNAP subsequently accumulates at the compartment, as seen in the bottom panel. A compartment that has recruited LC3B-SNAP like this will hereafter be referred to as *LC3-positive*.

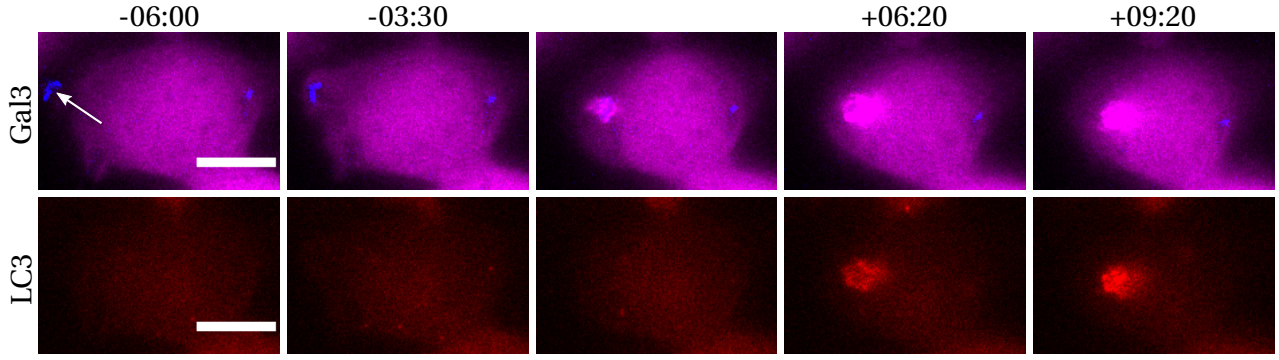

Figure 4.5: These images show a single cell that phagocytoses an *Mtb* mc^{2}6206, as indicated by an arrow in the first frame of the top panel. Subsequently, the bacterium-containing compartment becomes gal3-positive, suggesting phagosomal escape. The autophagy-associated protein LC3B accumulates at the gal3-positive site thereafter, as seen in the bottom panel. Scale bars equal 15 µm, and the time points relative to the middle frame are indicated above each column.

In total, 111 AGL-cells were infected with *Mtb* mc^{2}6206 and subsequently observed with TIRF microscopy. In these, there were 41 compartments that turned gal3-positive while being LC3B-negative, out of which 34 subsequently recruited LC3B. The remaining 7 gal3-positive

compartments either belonged to cells that lacked SNAP-expression (2 compartments), or did not visibly recruit LC3B within time of observation (5 compartments). Bacteria-containing compartments that recruited LC3B rapidly after entering the cell, with no preceding gal3 recruitment, were interpreted as LAP and are not included in this quantification.

Furthermore, 19 AGL-cells were stimulated with nanosilica and subsequently observed with TIRF microscopy. This resulted in 16 gal3-positive compartments in total, out of which 11 recruited LC3B. The remaining 5 gal3-positive phagosomes belonged to cells that lacked SNAP signal.

4.3.1 Recruitment of autophagy machinery to gal3-positive phagosomes possibly regulates ALG2 recruitment to the plasma membrane

Figures 4.6 and 4.7 show the LC3B-SNAP recruitment to gal3-positive compartments together with the ALG2-mNG signal in two *Mtb* mc^{2}6206-infected AGL-cells. In figure 4.6, LC3B-SNAP is accumulating at the gal3-positive compartment after some time, as seen in the third and fourth frame in the second panel. However, nothing happens in the ALG2-mNG TIRF channel. On the other hand, in figure 4.7, no LC3B-SNAP accumulation is seen to occur at the gal3-positive phagosome, and an ALG2 plasma membrane recruitment event occurs in the third frame. A movie of a *Mtb* mc^{2}6206-infected AGL-cell that displays both these features can be found by clicking or scanning the QR-code found in figure 4.8.

As these examples demonstrate, it seemed plausible from the imaging results that LC3B-recruitment to gal3-positive phagosomes was less prominent in cases where an ALG2-event occurred in the same spot as the compartment was located. The LC3B recruitment mostly appeared both slower and weaker for such compartments, as compared to compartments that was not related to any ALG2-events during the time of observation. It was especially interesting that gal3-positive phagosomes that became visible in the TIRF mode without inducing an ALG2-event usually were LC3B-positive.

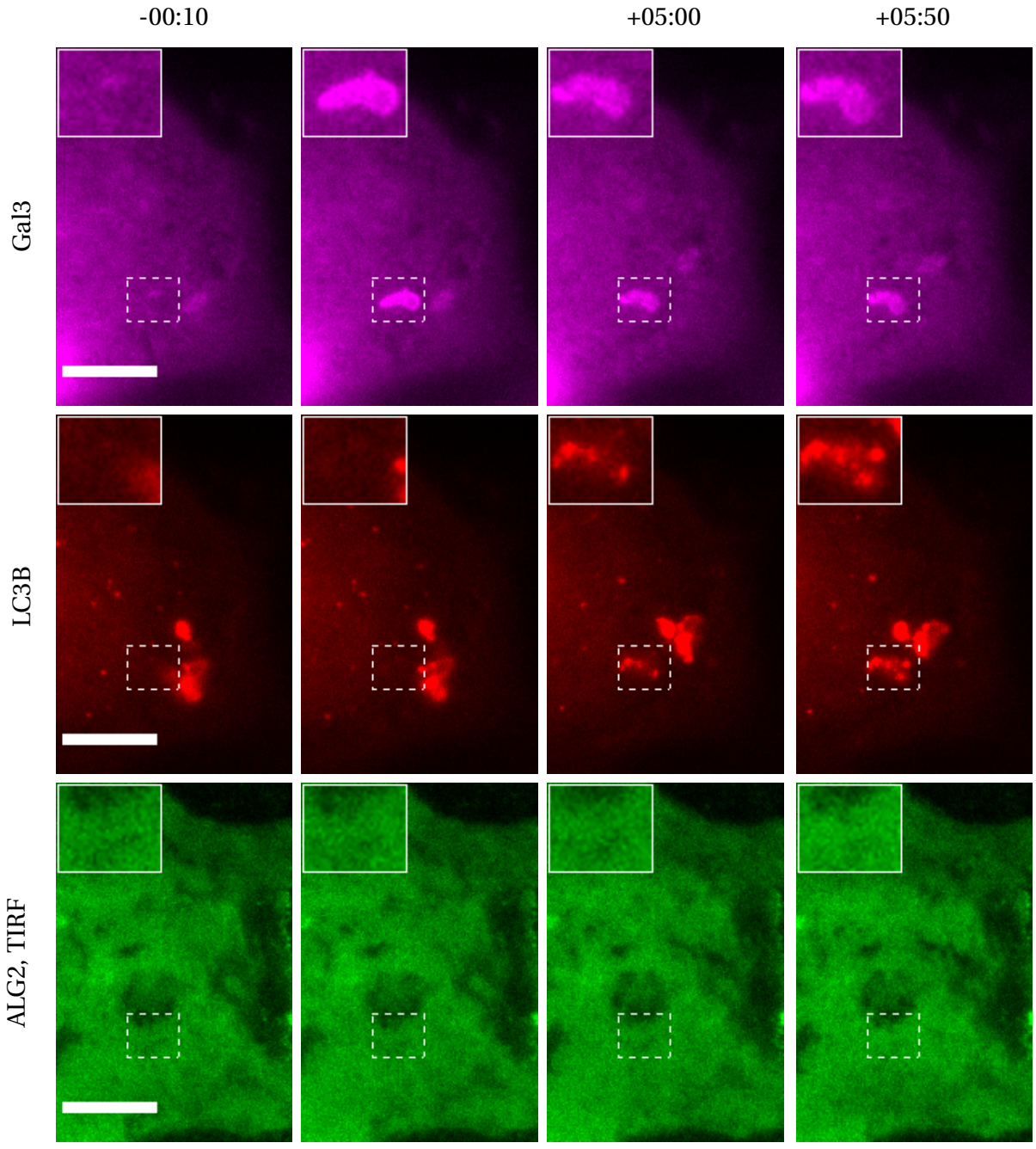

Figure 4.6: This figure shows the increase in LC3B-SNAP accumulation (second panel) at a compartment that become gal3-positive at time zero (first panel). The ALG2-mNG TIRF signal is shown in the bottom panel, and no event occurs. LC3B is recruited to the compartment over time, as is seen in the two last frames. For all panels, the scale bars equal 15 µm, and the time points relative to the compartment turning gal3-positive are indicated above each column. The relative time points are identical for this figure and figure 4.7. Insets show 2x magnifications of the dashed areas.

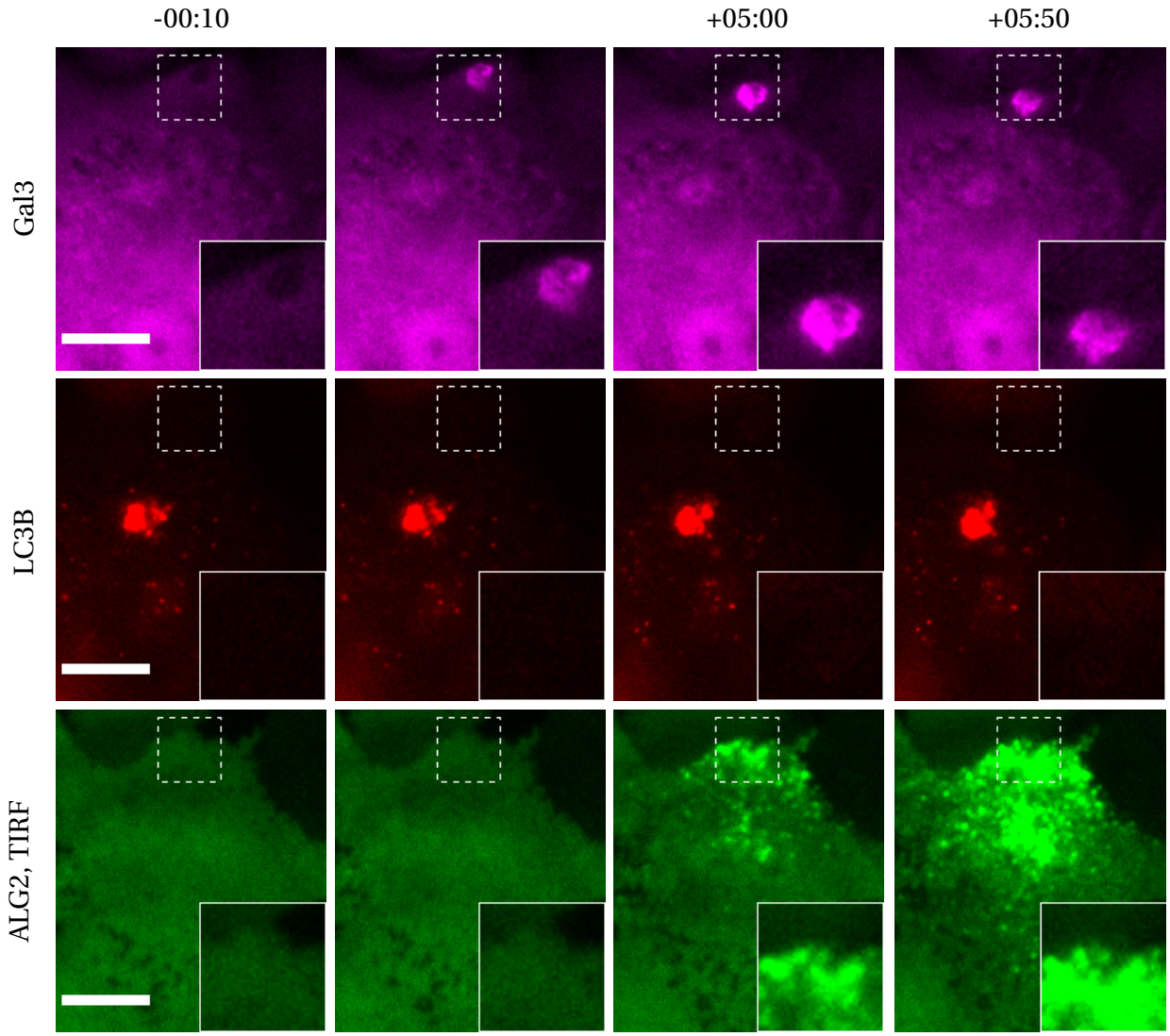

Figure 4.7: This figure, in comparison to figure 4.6, shows the LC3B-SNAP accumulation (second panel) at a compartment that become gal3-positive at time zero (first panel) and thereafter is related to an ALG2-event (bottom panel). Here, LC3B is not visibly recruited to the compartment. For all panels, the scale bars equal 15 µm, and the time points relative to the compartment turning gal3-positive are indicated above each column. The relative time points are identical for this figure and figure 4.6. Insets show 2x magnifications of the dashed areas.

Figure 4.8: By scanning or clicking the above QR-code, the reader follows a link to a movie of events similar to those shown in figures 4.6 and 4.7. Here, a single cell with two *Mtb* mc^{2}6206-containing compartments is displayed. Both compartments turn gal3-positive (middle), but only one of them recruits LC3B (right). The compartment that does not recruit LC3B is at the same site as an ALG2 plasma membrane recruitment event seen in TIRF mode (left).

Image analysis: LC3B recruitment to two different categories of gal3-positive vesicles

To quantify the LC3B recruitment, ROIs were drawn around gal3-positive, LC3B-negative phagosomes in two categories: ALG2-event-related compartments, and compartments that seem unrelated to ALG2. There were ten compartments of each kind. The LC3B mean gray value development in the ROIs was then measured, and aligned to the event of the compartment turning gal3-positive. The measurements were thereafter normalized to the respective first frame of a range around the event. The median and interquartile range of the two data sets were plotted with GraphPad, and the result is shown in figure 4.9. As is seen in the plot, the compartments that are not associated with an ALG2 plasma membrane event does indeed seem to recruit LC3B more strongly. At time points 7.5, 10 and 12.5 minutes after the vesicle turns gal3-positive, the difference is significant ($p < 0.05$ at time points 7.5 and 12.5 minutes, $p < 0.01$ at time point 10 minutes) according to the two-tailed Mann-Whitney *U* test.

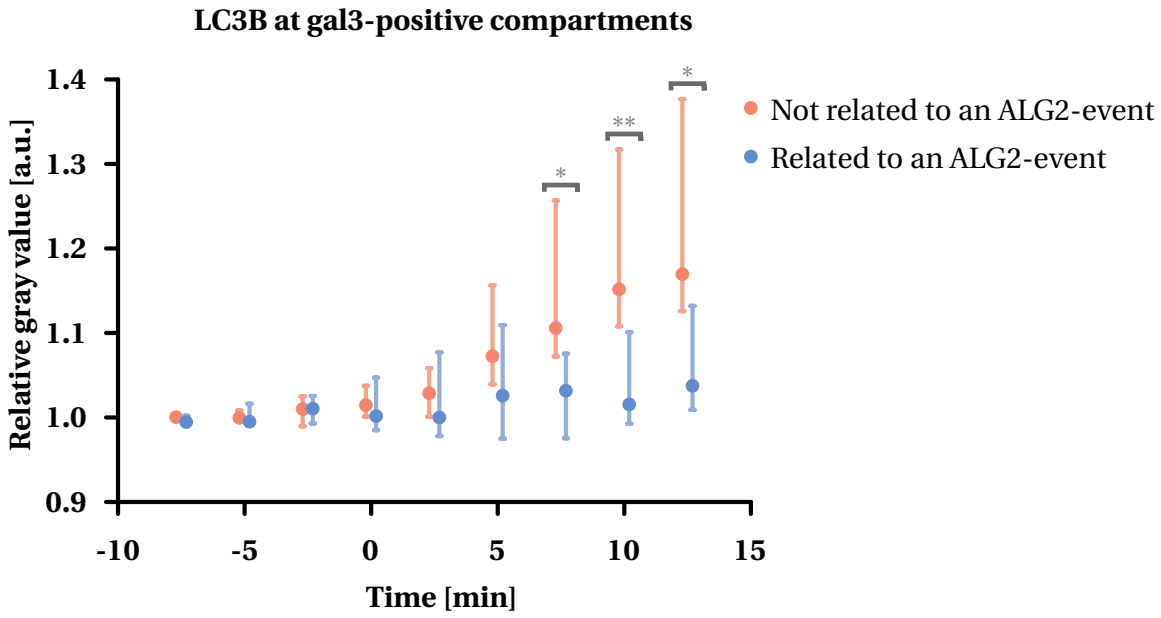

Figure 4.9: This plot shows the increase in LC3B-SNAP gray value at sites that become gal3-positive at time zero. Red dots indicate measurements of gal3-positive compartments that are unrelated to ALG2. Blue dots indicate measurements of gal3-positive compartments that are related to ALG2 recruitment events at the plasma membrane. Both plots show median and interquartile range of measurements for ten separate gal3-events. The difference between the two categories is significant at the three last time points, according to the two-tailed Mann-Whitney *U* test.

4.3.2 Autophagy inhibition does not increase ALG2 recruitment to the plasma membrane

To further examine whether autophagy indeed affects ALG2-events at the plasma membrane, the next step was to inhibit autophagy by loading the cells with the ULK1/2 inhibitor MRT before and during infection with *Mtb* mc^{2}6206. This should dampen xenophagy, while LAP is independent of ULK1 and should therefore not be affected. The response was recorded by TIRF and widefield fluorescence microscopy time-lapse imaging for approximately 2 hours post-infection.

Image analysis: Autophagy inhibition with MRT

To analyze the autophagy inhibition results, ROIs were drawn around gal3-positive, LC3B-negative phagosomes, and the mean gray value of the LC3B signal was measured. The measurements were aligned to the event of the compartment turning gal3-positive, and thereafter normalized to the respective first frame of a certain range around the event. Thereafter, the median and interquartile range of the data set was plotted with GraphPad. The result is displayed in fig-

ure 4.10. The measurements from cells that have not been treated with MRT are shown as blue dots, and data from cells that have been treated with 2 µM MRT are red. It seems evident that recruitment of LC3B to bacteria-containing compartments happens earlier in cells that are not autophagy-inhibited, due to the greater LC3B gray value in these images – suggesting that the inhibition was successful for some time, and autophagy was delayed. At time points 10 and 15 minutes after the vesicle turns gal3-positive, the difference is significant ($p < 0.05$) according to the two-tailed Mann-Whitney *U* test.

Cells that were treated with 5 µM MRT seemed to suffer from toxic effects, and the results were discarded. Due to time limitations, no other concentrations were tested and the experiments could not be repeated.

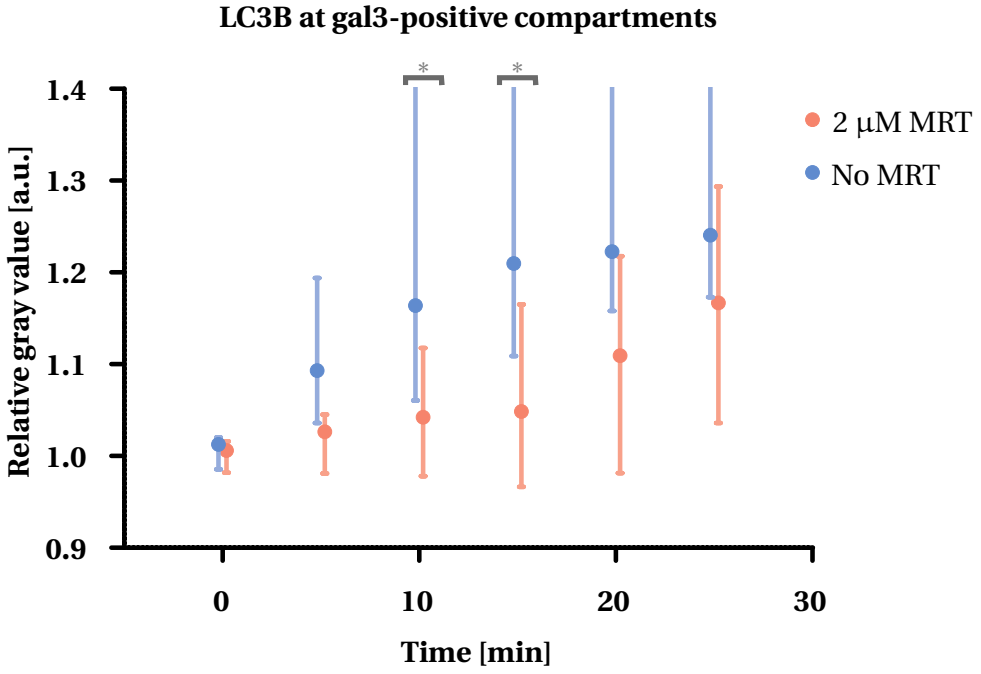

Figure 4.10: This plot shows the increase in LC3B-SNAP gray value at sites that become gal3-positive at time zero. Blue dots indicate measurements of gal3-positive compartments in cells under normal conditions. Red dots indicate measurements of gal3-positive compartments in cells that was inhibited with 2 µM MRT. The use of this inhibitor apparently delays the onset of LC3B recruitment, as the increase in LC3B-SNAP gray value is slower for these measurements. Both plots shows median and interquartile range of measurements for ten separate and independent gal3-events, and all measurements have been normalized to the first frame in the respective data sets. The difference between the two categories is significant at the two middle time points, according to the two-tailed Mann-Whitney *U* test.

However, the seemingly successful autophagy inhibition did not affect the amount of large ALG2-events at sites of gal3-positive phagosomes. As mentioned above, 111 AGL-cells were in-

fected with *Mtb* mc^{2}6206 and observed under normal conditions, and this resulted in 41 gal3-positive phagosomes and 10 large, local ALG2-events. On the other hand, 41 AGL-cells were infected and observed with 2 µM MRT in the medium. In these experiments, there were 34 gal3-positive phagosomes, and 8 large, local ALG2-events. It does seem like the uptake was higher with the autophagy-inhibited cells, which could be due to fresher serum or other experimental circumstances. Nevertheless, the fraction of gal3-events that relates to ALG2-events seems unchanged.

4.3.3 Autophagy protein knockdown possibly affects ALG2 recruitment to the plasma membrane

Furthermore, ATG-5 knockdown AGL-cells were also infected with *Mtb* mc^{2}6206. The medium in the wells were exchanged for a colored bacteria suspension with an OD of 0.04-0.05. Thereafter, the cells were observed with TIRF and widefield fluorescence microscopy time-lapse imaging for approximately 2 hours post-infection. This was done in order to address how autophagy affects ALG2-events at the plasma membrane in a more precise manner than by using an inhibitor, as MRT only seemed to delay the onset of xenophagy. However, the bacterial uptake was unusually low, possibly due to the fact that the serum that was used had been thawed too many times and consequently lost its complement activity. It was therefore only 3 gal3-events in 27 observed cells, and no ALG2-events. No conclusions could thus be made. The experiments could not be repeated due to time constraints.

4.4 Consequences of membrane damage for NLRP3 inflammasome activation

Figure 4.11 shows a single AGA-cell that has been infected with *Mtb* mc^{2}6206 and as a result gets an ASC speck and dies through pyroptosis. Prior to the ASC speck formation, the cell displays plasma membrane recruitment of ALG2, shown in the inset in the second frame of the first panel.The speck thereafter starts to form, as indicated by an arrow in the third frame of the second panel. Finally, the pyroptotic morphology of swelling and a more prominent nucleus is seen in the brightfield channel, as indicated by an arrow in the last frame of the bottom panel.

In the employed ASC-mIRFP670-expressing cell lines during both nanosilica treatment and *Mtb* mc^{2}6206 infection, there was a total of 41 specks formed. Out of these, 26 formed in cells that displayed a pre-speck ALG2 plasma membrane recruitment event. In cells that were stimulated with nanosilica (143 cells), 10 specks formed, out of which 9 came subsequent to an ALG2-event. For *Mtb* mc^{2}6206-infected cells (136 cells), formation of 31 specks was registered, out of

which 17 came after an ALG2-event. Evidently, there seems to be more speck formation during *Mtb* mc^{2}6206 infection.

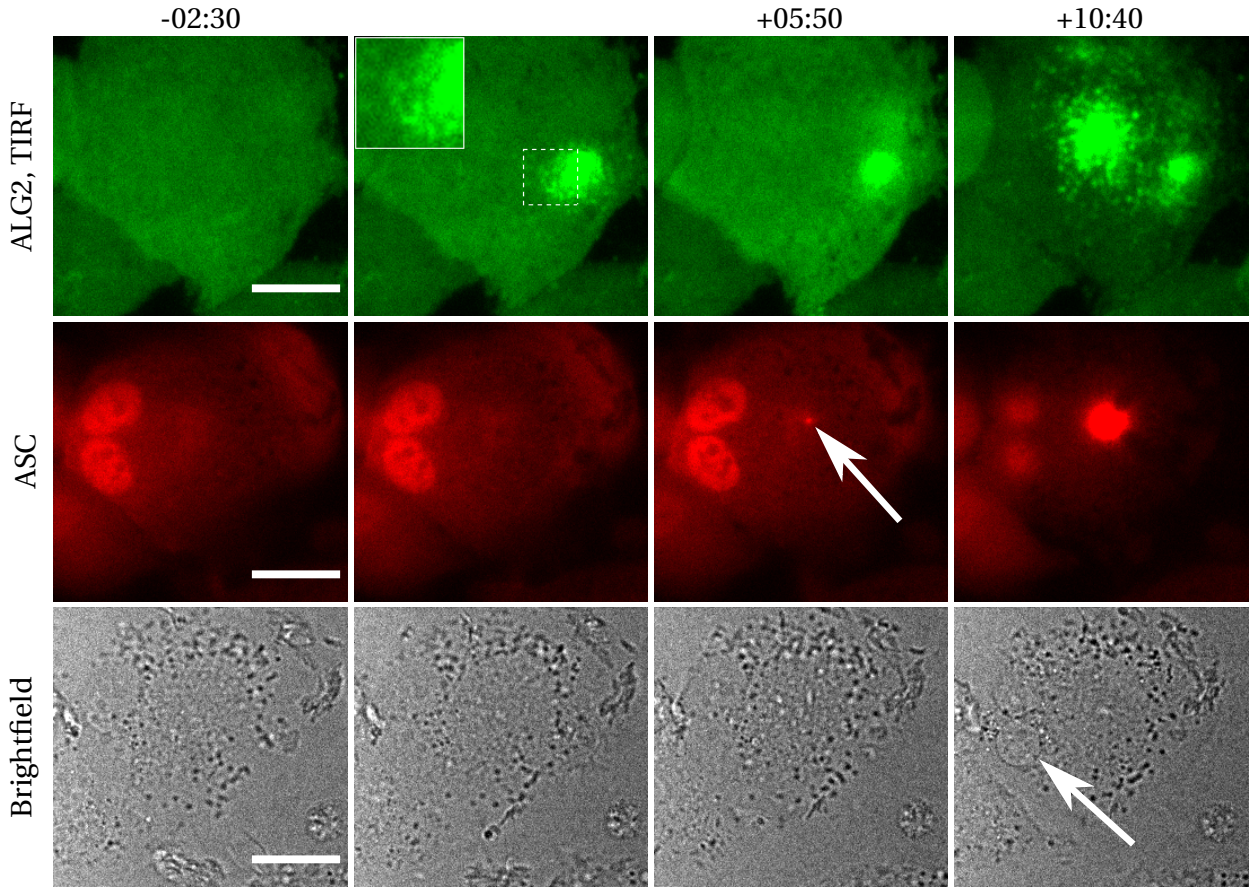

Figure 4.11: This figure shows ASC speck formation and pyroptotic morphology in a single cell is infected with *Mtb* mc^{2}6206 and has an ALG2 plasma membrane event. The upper panel shows the ALG2-mNG TIRF signal, the second panel shows the ASC-mIRFP670 widefield signal and the bottom panel shows the brightfield signal. Scale bars equal 20 µm, and the timepoints relative to the second frame are indicated above each column. Insets show 2x magnifications of the dashed areas. The ALG2-mNG TIRF signal shows plasma membrane recruitment of ALG2 in the second frame, as a result of *Mtb* mc^{2}6206 uptake. The ASC-mIRFP670 signal shows formation of a speck in the third frame, indicated by an arrow. Lastly, the brightfield images show pyroptotic morphology in the last frame, also indicated by an arrow.

4.5 ALG2 recruitment to the plasma membrane is accompanied by a calcium flux, while gal3-events are not

How calcium fluxes in the cell relate to ALG2- and gal3-events could possibly uncover more details about their interplay, or the mechanisms behind the events. Furthermore, examining the presence of ion fluxes during ALG2 plasma membrane recruitment is an interesting endeavor in relation to NLRP3 activation, as ion fluxes clearly play a role, but the details are disputed.

Thus, to examine the relationship between ion fluxes and cellular events that occur during NLRP3 stimuli and *Mtb* $mc^2$6206 infection, AA- and AG-cells were loaded with the calcium indicator probe Calbryte 590 AM (hereafter referred to as Calbryte) for one hour before experiments, and observed by fluorescence microscopy during stimuli or infection.

In this system, an intensity increase in the channel excited by the 561 nm laser should correspond to a influx of Ca^{2+} to the cytosol.

4.5.1 Imaging of Calbryte intensity changes

Verification of the system: ATP treatment

To verify the system, cells were treated with ATP, which causes a ion channel calcium influx after binding to the ligand-gated P2X7 receptor [75]. Figure 4.12 shows images of a single cell, loaded with Calbryte, that has been treated with 3 mM ATP. The top panel shows the ALG2-mNG signal in TIRF, and the bottom panel shows the widefield Calbryte signal. Time points after the second frame are indicated above the columns. As can be seen in the second ALG2-mNG frame, a weak and transient dot pattern appears in the very beginning of the experiment. At the same time point, the Calbryte intensity is seen to increase, indicating a calcium flux.

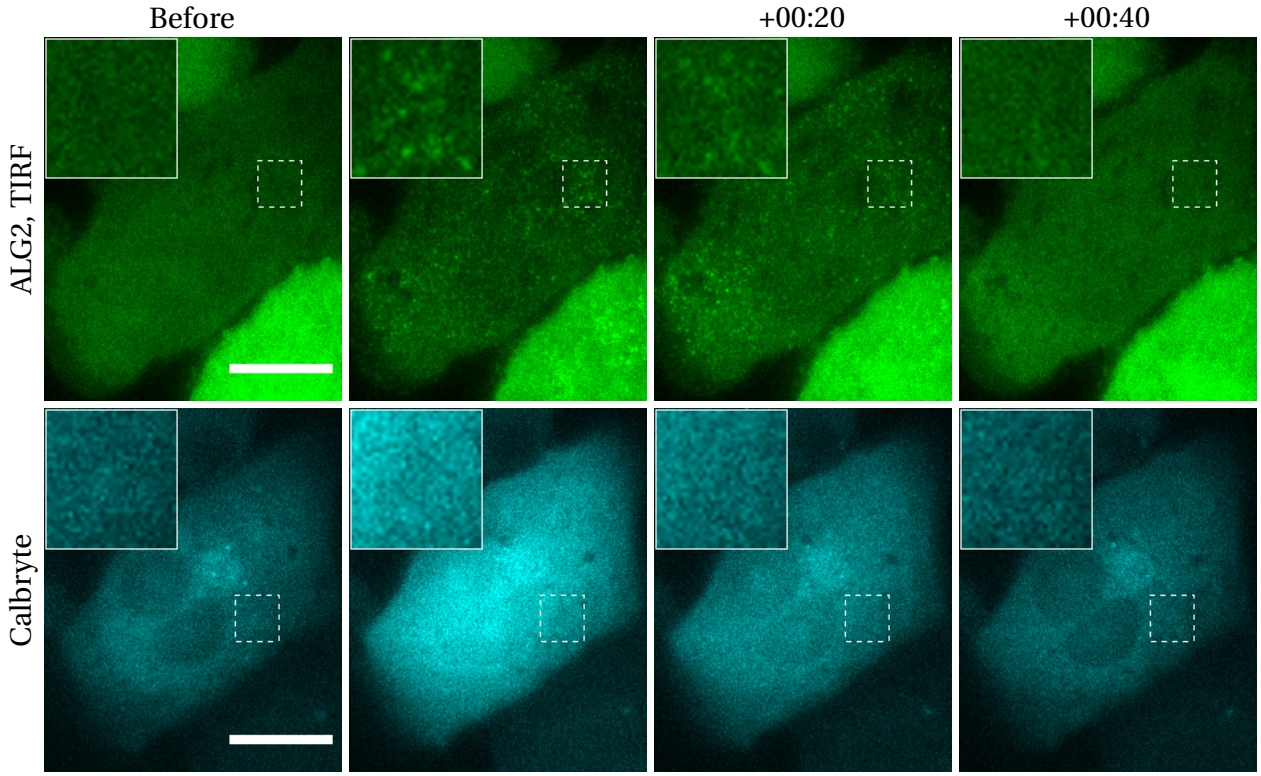

Figure 4.12: This figure shows the development of Calbryte intensity (lower panel) in a cell as it is treated with 3 mM ATP, causing a weak and transient ALG2 recruitment to the membrane (upper panel), as seen in the insets. Scale bars equal 20 µm, and the timepoints relative to the second frame are indicated above each column. Insets show 3x magnifications of the dashed areas.

Verification of the system: Saponin treatment

For further verification that the calcium reporter was successful, the Calbryte system was also tested with the glycoside saponin, which causes formation of plasma membrane pores [76]. Such pores should allow influx of extracellular calcium. The results are depicted in figure 4.13. The top panel shows the ALG2-mNG signal in TIRF, and the bottom panel shows the widefield Calbryte signal. The time points after the leftmost frame are indicated above each column, and the insets show 2x magnifications. Due to the damage to the plasma membrane, calcium influx happens, as seen in the intensity changes of the Calbryte signal. These fluxes coincide with ALG2 recruitment to the plasma membrane, as shown in the starry patterns in the upper panel. The process was significantly slower than the ATP response, which is as expected, as saponin induces real damage, while ATP opens channels.

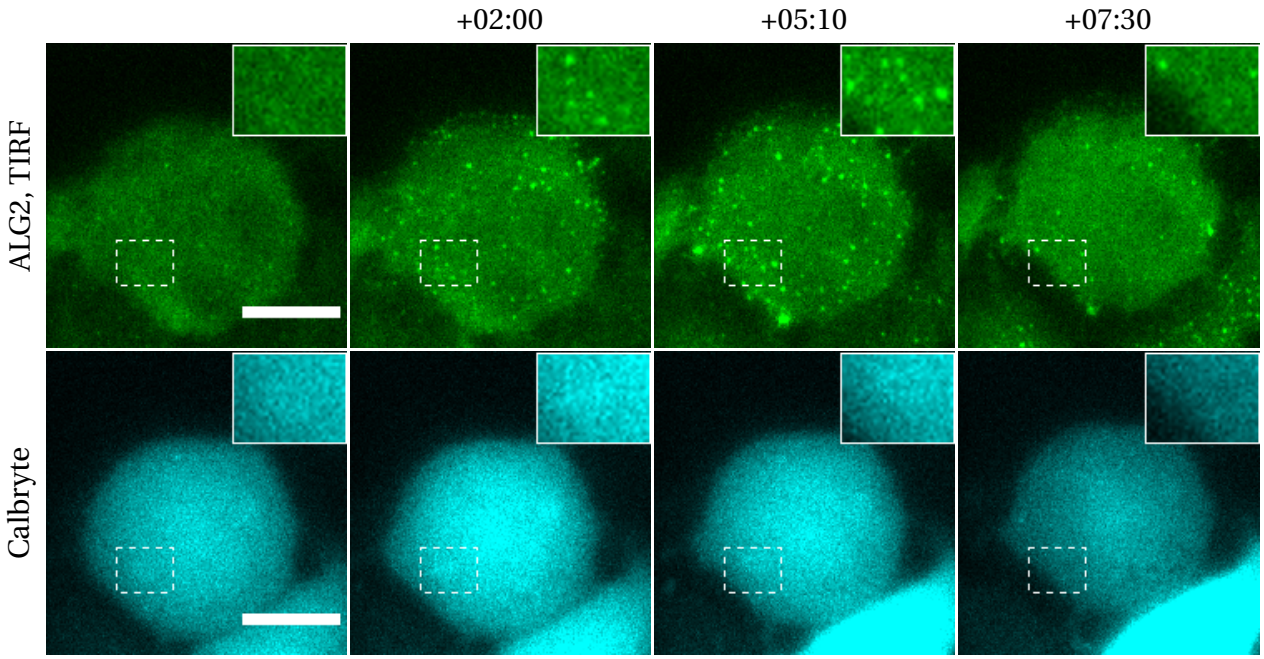

Figure 4.13: This figure shows the development of Calbryte intensity (lower panel) in a cell as it is treated with 0.05% saponin, causing ALG2 recruitment to the membrane (upper panel). Scale bars equal 15 µm, and the timepoints are indicated above each column.

Calcium flux response to nanosilica treatment

To examine how the calcium fluxes change during exposure to nanosilica and how this relates to ALG2 recruitment to the plasma membrane, Calbryte-loaded cells were stimulated with 200 µg/ml nanosilica in complete RPMI and studied with fluorescence microscopy time-lapse imaging for approximately 2 hours, starting 1-6 hours after the stimuli. The results are shown in figure 4.14. The top panel shows the ALG2-mNG signal in TIRF, and the bottom panel shows the widefield Calbryte signal. Time points relative to the second frame are indicated above each column. As is evident, the ALG2-recruitment to the plasma membrane increases over time and coincides with a calcium flux in the cell.

In total, 55 AA-cells were observed under these conditions. 29 of these displayed pre-speck ALG2 membrane recruitment.

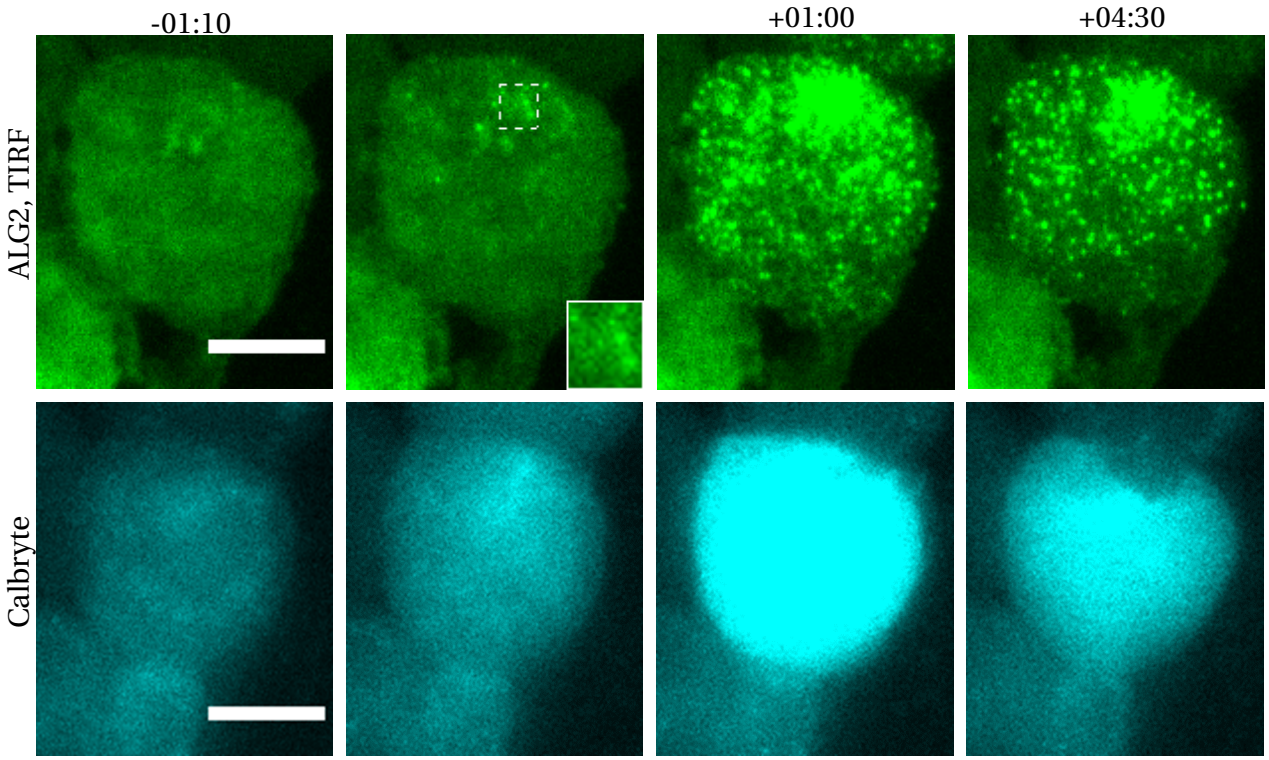

Figure 4.14: This figure shows the development of Calbryte intensity (lower panel) in a cell simultaneously as a pre-speck ALG2-event (upper panel) occurs after treating the cells with nanosilica. Scale bars equal 15 µm, and the timepoints before and after the ALG2-event are indicated above each column. Insets show 2x magnifications of the dashed areas.

Figure 4.15 shows the quantification of the Calbryte intensity development in cells that have been treated with nanosilica and as a result has ALG2-events. ROIs were drawn in crosstalk-free areas in the Calbryte channel images of cells that displayed ALG2 plasma membrane recruit-

ment events. The mean gray value in the ROIs were thereafter measured in all images. Ten cells were used for the analysis. The data was aligned so that the ALG2-event happens at time zero, and the measurements were normalized to the respective first frame of the chosen data set range. The measurements were thereafter plotted with GraphPad. As can be seen in the plot, ALG2-events are clearly associated with a rapid increase in mean gray value in the Calbryte channel, indicating a calcium flux.

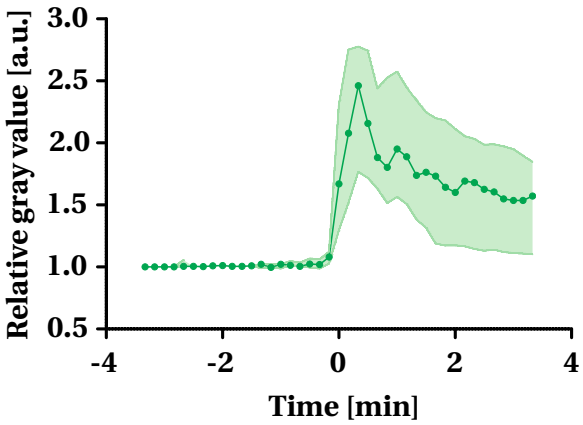

Figure 4.15: This plot shows the median of the relative gray value of the Calbryte signal in ten individual cells over time. The cells were treated with nanosilica and display pre-speck ALG2-recruitment to the plasma membrane. The datasets have been aligned so that the ALG2-event is first detectable at timepoint zero. Interquartile range is indicated by the colored area. The measurements are normalized to the value from the first frame in each data set.

Calcium flux response to *Mtb* mc^{2}6206 infection

Furthermore, it was studied how calcium fluxes change during *Mtb* mc^{2}6206 infection, and how this related to plasma membrane recruitment of ALG2. Calbryte-loaded cells were infected with the bacterium by exchanging the medium in the wells with a suspension of colored *Mtb* mc^{2}6206 at an OD between 0.04 and 0.05. Subsequently, the cells were examined with fluorescence microscopy time-lapse imaging for approximately 2 hours after infection. The results are shown in figure 4.16. The ALG2-mNG signal in TIRF is shown in the upper panel, and the widefield Calbryte signal is shown in the bottom panel, while the time points relative to the second frame are shown above each column. As is shown in the images, ALG2 is recruited to the plasma membrane and is accompanied by an increase in Calbryte intensity. A movie which shows the dynamics of this event more clearly can be found by clicking or scanning the QR-code found in figure 4.17. In addition to the Calbryte intensity fluxes that seemed to be associated with ALG2 plasma membrane recruitment, more transient fluxes occurred regularly, commonly seen as intensity increases that lasted for one or two frames. This was as expected, as increases in the

calcium level in the cytosol is part of several signaling events. Furthermore, when the cells died, both after ALG2 plasma membrane recruitment events and in general, a large Calbryte intensity increase was seen. Very shortly after, the Calbryte signal disappeared from the cell, leaving behind some debris in bright compartments. This can be explained by how there would be a very large calcium influx to the cell at the moment the plasma membrane loses its integrity, and thereafter, diffusion of Calbryte should occur.

In total, 52 AA-cells were observed under these conditions. 16 of them displayed ALG2 plasma membrane recruitment prior to speck formation.

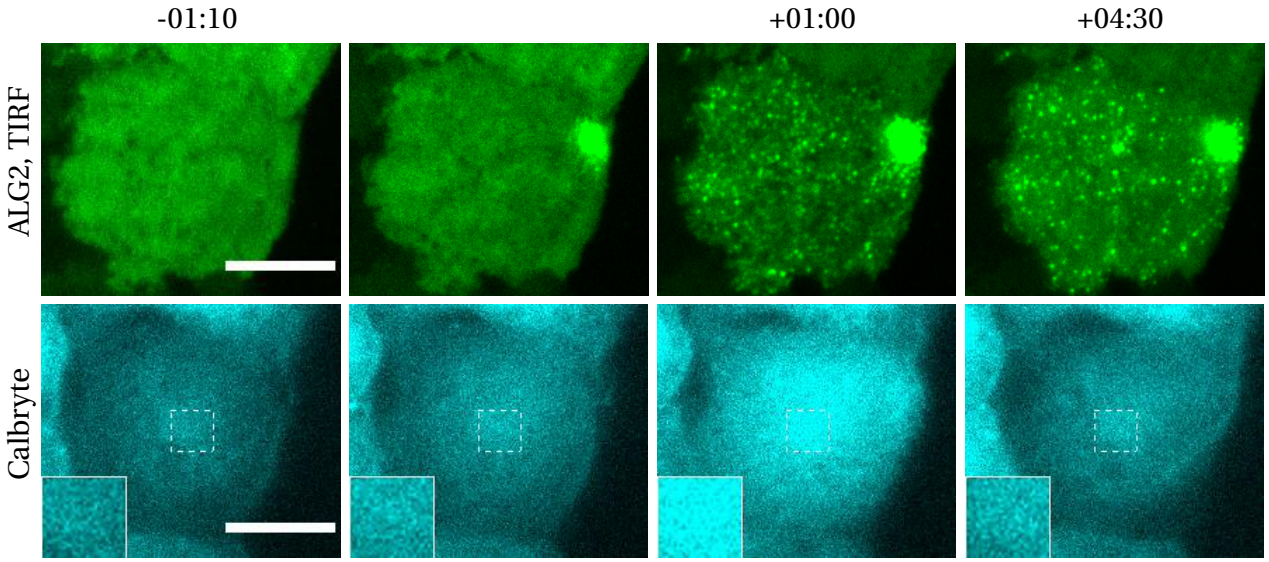

Figure 4.16: This figure shows the development of Calbryte intensity (lower panel) in a cell simultaneously as a pre-speck ALG2-event (upper panel) occurs after infecting the cells with *Mtb* $mc^2$6206. Scale bars equal 20 µm, and the timepoints before and after the ALG2-event are indicated above each column. Insets show 2x magnifications of the dashed areas.

Figure 4.17: By scanning or clicking the above QR-code, the reader follows a link to a movie of the events shown in figure 4.16.

To examine whether or not the event of the bacterium-containing vesicle turning gal3-positive is related to a calcium flux, Calbryte-loaded AG-cells were infected with *Mtb* mc^{2}6206 by exchanging the medium in the wells for a colored *Mtb* mc^{2}6206 suspension with an OD of 0.04-0.05. Subsequently, the cells were observed with fluorescence microscopy time-lapse imaging for approximately 2 hours. The results are shown in figure 4.18. The widefield gal3-mSc signal is shown in the upper panel, and the widefield Calbryte signal is shown in the bottom panel. The time points relative to the second frame are shown above each column. It seems that gal3-events are not accompanied by an increase in Calbryte intensity.

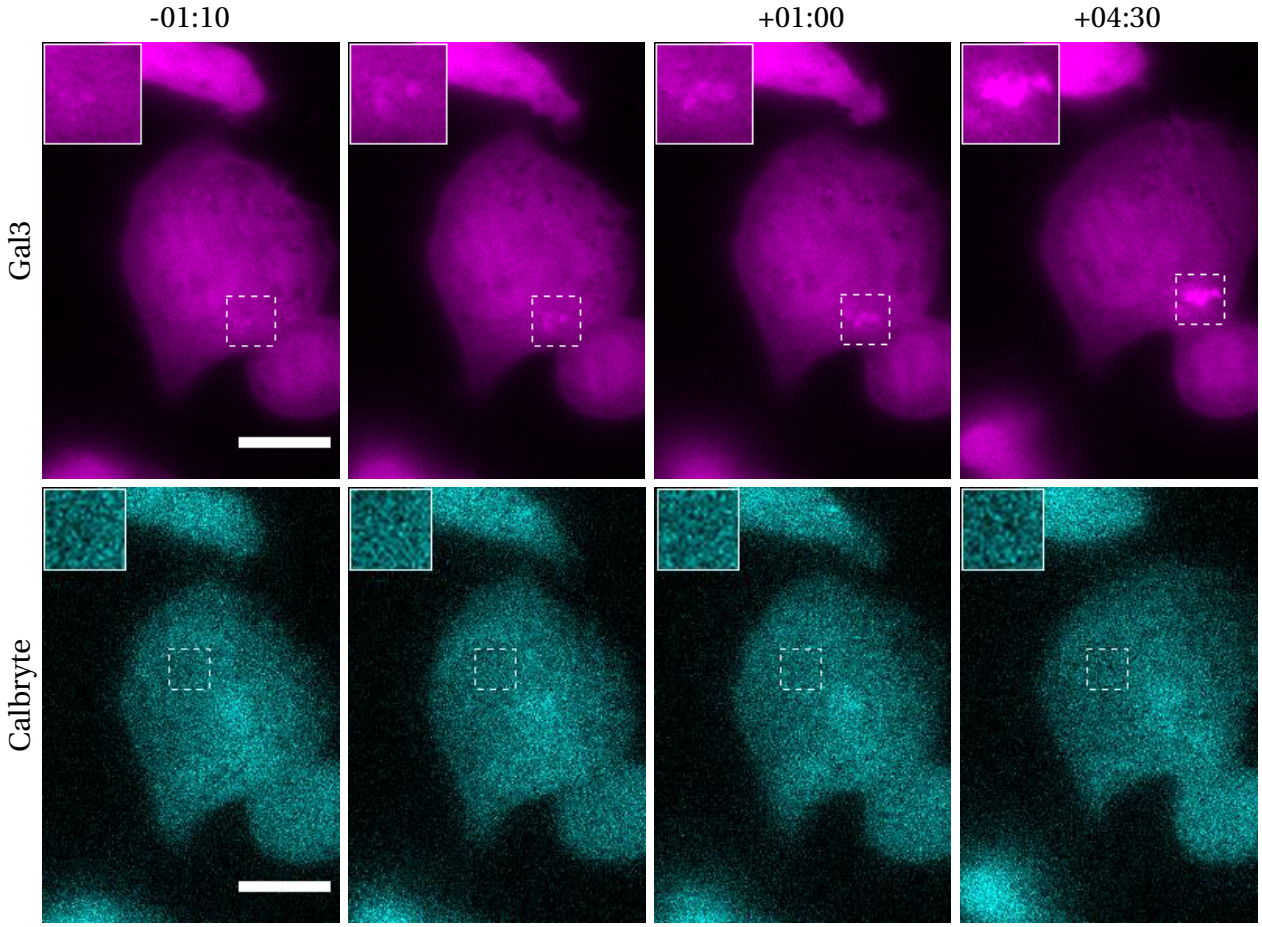

Figure 4.18: This figure shows the development of Calbryte intensity (lower panel) in a cell simultaneously as a gal3-event (upper panel) occurs after infecting the cells with *Mtb* mc^{2}6206. Scale bars equal 15 µm, and the timepoints before and after the gal3-event are indicated above each column. Insets show 2x magnifications of the dashed areas.

Figure 4.19 shows the quantification of the development of the Calbryte intensity in cells that have been infected with *Mtb* mc^{2}6206 and as a result get ALG2 plasma membrane recruitment events and compartments that turn gal3-positive. Ten independent events were used for

both analyses. ROIs were drawn in the images from the Calbryte channel, in crosstalk-free areas within cells that displayed events of interest. The mean gray value in the ROIs were thereafter measured in all images. The data was aligned so that the ALG2-event happens at time zero in figure 4.19 a) and the gal3-event happens at time zero in figure 4.19 b), and the measurements were normalized to the respective first frame of the chosen data set range. The measurements were thereafter plotted with GraphPad. As is clear from the plots, ALG2-events are associated with a rapid increase in mean gray value in the Calbryte channel, indicating a calcium flux, while the gal3-events are not.

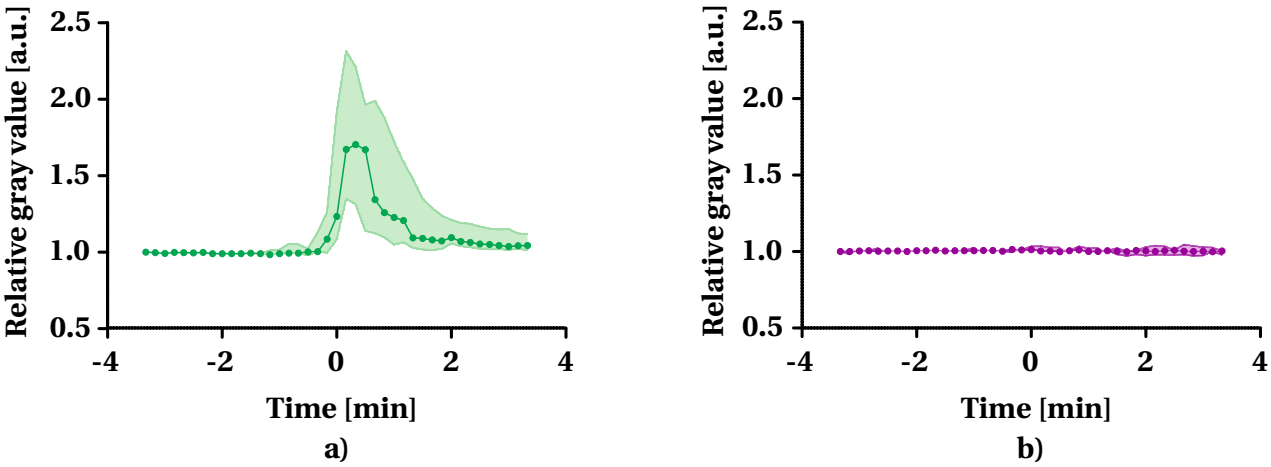

Figure 4.19: Each of these plots shows the median of the relative gray value of the Calbryte signal at sites of ten individual events over time. The cells have been infected with *Mtb* $mc^2$6206. Interquartile range is indicated by the colored area. The measurements are normalized to the gray value of the first frame in each data set. **a)** Here, the Calbryte development in cells that display pre-speck ALG2-recruitment to the plasma membrane is plotted. The datasets have been aligned so that the ALG2-event is first detectable at timepoint zero. **b)** Here, the Calbryte development in cells that display a gal3-event is plotted. The datasets have been aligned so that the gal3-event is first detectable at timepoint zero.

4.6 Control experiments

Several control experiments were performed to ensure reliable results.

4.6.1 Untreated cells

During time-lapse imaging of AGA-cells for 45 minutes with no stimuli, no changes occurred in neither ALG2-mNG in TIRF, ALG2-mNG in widefield, Gal3-mSc in TIRF, Gal3-mSc in widefield, ASC-mIRFP670 in widefield nor brightfield (not shown).

4.6.2 Treatment with 0.05% saponin

The pore-forming toxin saponin was used as a control to ensure that membrane damage indeed does show up as bright ALG2-mNG punctae in the TIRF channel. Figure 4.20 shows the result of treating the cells with 0.05% saponin.

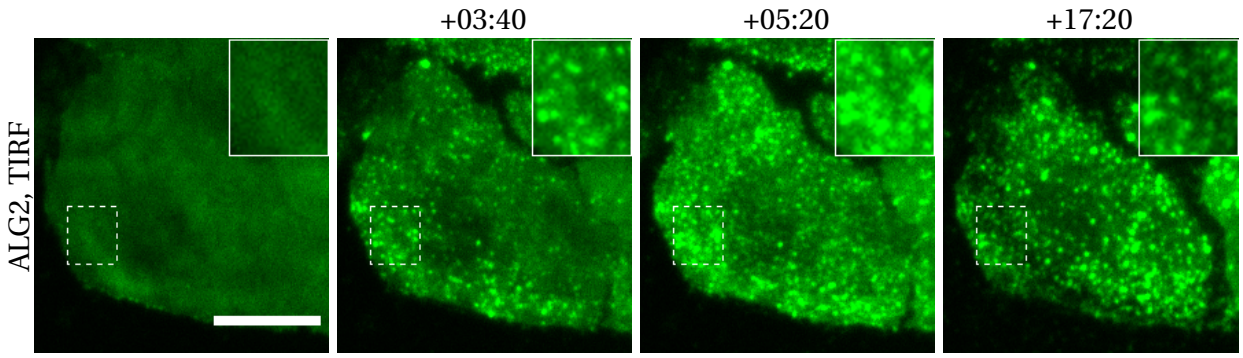

Figure 4.20: This image shows the ALG2-mNG TIRF signal from a single cell that has been treated with 0.05% saponin. The scale bar equals 20 µm and the time points after the first frame are indicated above. The insets show 2x magnifications of the dashed areas.

4.6.3 Calbryte-loaded cells over time with no stimuli

To examine the baseline for calcium flux in cells with no stimuli, cells were loaded with Calbryte for 1 hour, washed with complete RPMI, and subsequently observed over time. Transient Calbryte intensity changes occurred approximately to the same degree as during nanosilica treatment and *Mtb* $mc^2$6206 infection, but these were smaller relative intensity changes in the control cells. No large fluxes were seen. Such a control cell is shown in figure 4.21.

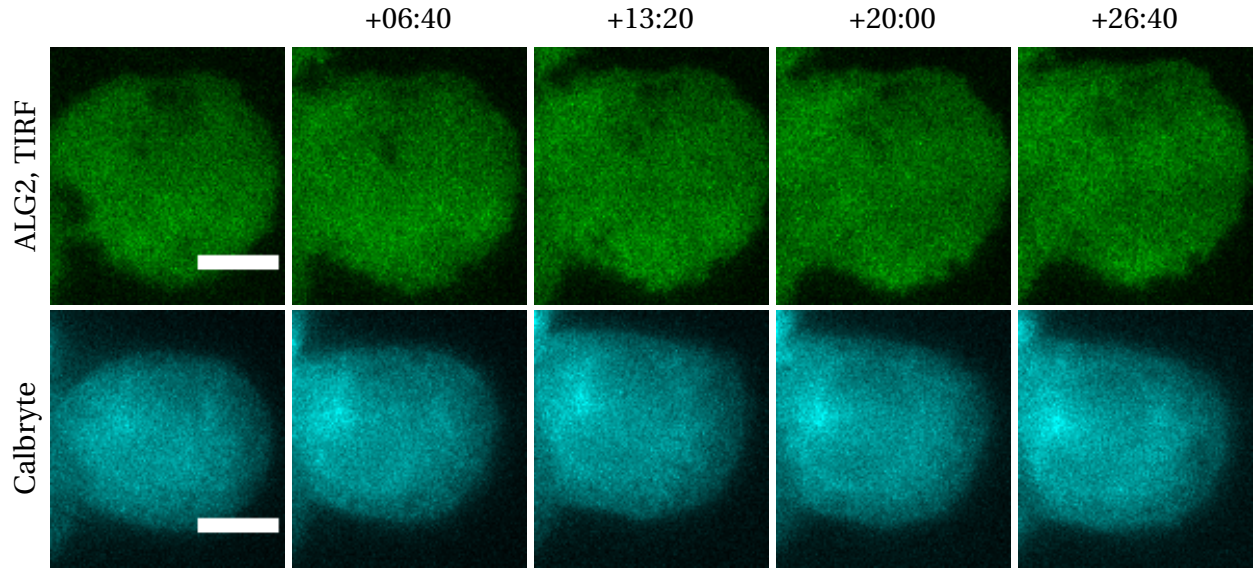

Figure 4.21: These images show the ALG2-mNG TIRF signal and the Calbryte widefield signal from a single cell that has not been stimulated in any way. The scale bar equals 10 µm and the time points after the first frame are indicated above.

4.6.4 Treatment with $TPCS_{2a}$

$TPCS_{2a}$ is a compound that localizes to endomembranes and locally disrupts these when activated through illumination [77]. The cells were loaded with this photosensitive chemical in order to damage lysosomal compartments through a distinct route and compare the effects.

Before activation of the compound, the cells were imaged with TIRF and widefield fluorescence microscopy. After activation, the cellular response was recorded with fluorescence microscopy time-lapse imaging, capturing a new frame every 30 seconds. The results are presented in figure 4.22. As is evident in the images, gal3-positive compartments start to show up after some time, indicating damage to lysosomal compartments. However, no response is seen in the ALG2-mNG TIRF channel or the LC3B channel. This suggests that inflicting lysosomal damage through this chemical route is different from the damage mediated by nanosilica and *Mtb* $mc^2$6206.

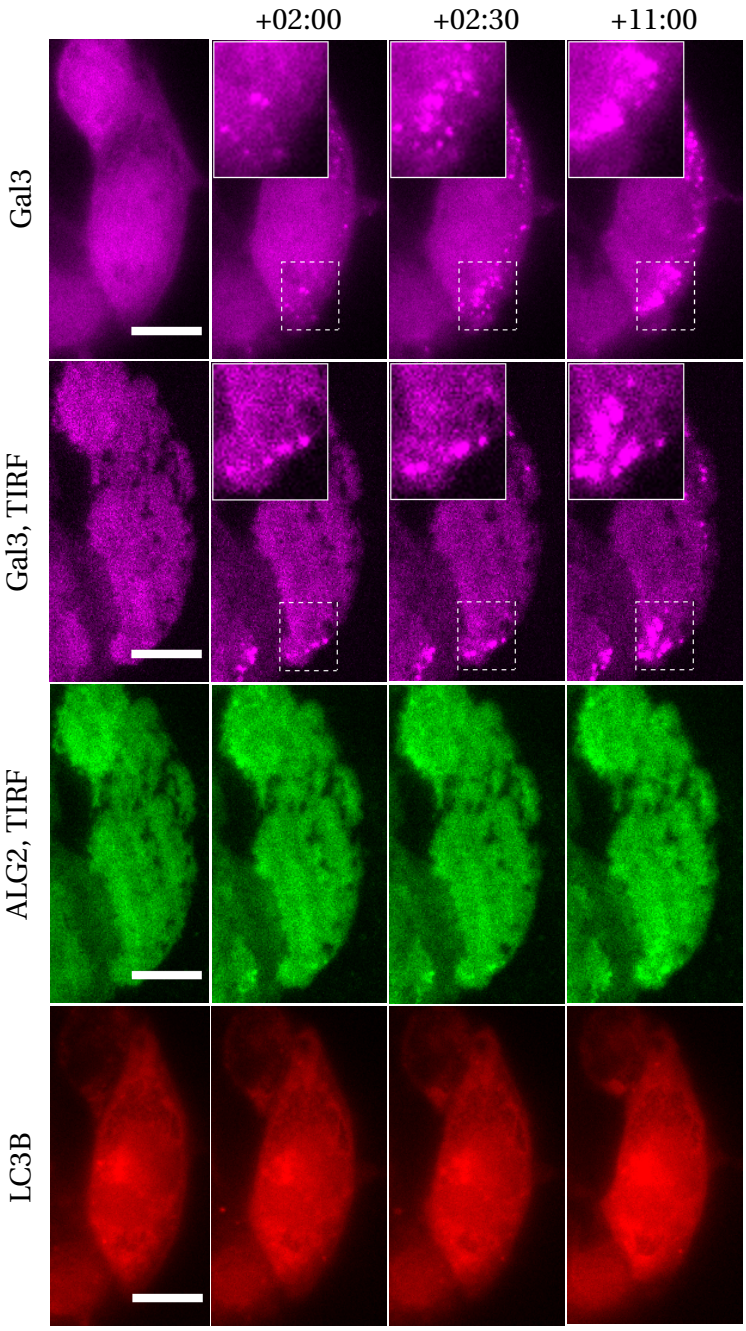

Figure 4.22: This image shows the gal3-mSc widefield and TIRF signal (top and second panel, respectively), ALG2-mNG TIRF signal (third panel) and LC3B-SNAP signal (bottom panel) from a single cell that has been loaded with $TPCS_{2a}$ and illuminated with the 405 nm laser line at 10% power for a duration of 1 second for activation of the compound. The scale bar equals 15 µm and the time points after the first frame are indicated above each column. The insets show 2x magnifications of the dashed areas.

Chapter 5

Summary and discussion

In the work presented in this thesis, cell lines expressing various fluorescent proteins have been stimulated with nanosilica and infected with *Mtb* mc^{2}6206, and subsequently studied with TIRF microscopy. The dynamics of the membrane repair-associated protein ALG2, phagosomal escape marker gal3, inflammasome indicator ASC and autophagy-related protein LC3B have been examined with fluorescence microscopy. Their relation to calcium fluxes was also studied, by the use of the fluorescent probe Calbryte. It was seen that in many cases (approximately 55%), ALG2-recruitment to the plasma membrane happened in large, local accumulations at the same position as a gal3-positive phagosome. In some experiments, the compartment could even be seen in the TIRF mode, implying that it was close to the plasma membrane. The cells died through pyroptosis, after formation of an ASC speck. Furthermore, LC3B was found to be recruited to gal3-positive phagosomes. It was a stronger recruitment to compartments that were unrelated to an ALG2-event. Inhibition of autophagy seemingly did not affect the amount of ALG2 recruitment to the plasma membrane, and preliminary experiments with ATG-5 knockout cells were inconclusive. Lastly, it was found that ALG2-recruitment to the plasma membrane was associated with a calcium flux both in cases of nanosilica treatment and *Mtb* mc^{2}6206 infection. Cases of mycobacterium-containing compartments turning gal3-positive was not associated with a calcium flux.

5.1 Experimental procedures

All experiments reported in this thesis employed TIRF microscopy on live cells. The objective and camera on the specific microscope allowed observation of an area approximately 130 µm x 130 µm large. Tiling was not possible due to problems with the autofocus when using this setting. Consequently, one session of time-lapse imaging usually allowed observation of around 5-15 cells. Considering that each set of cells were observed for approximately 2 hours, this is quite a low throughput. Nevertheless, the obtained information is unique, as observation of events occurring at or near the plasma membrane is enabled. A higher throughput (and greater resolution) could be obtained by the use of other microscopy techniques such as confocal microscopy with a lower magnification, but this would be at the cost of the membrane sensitivity.

5.2 The interaction between gal3 and ALG2

The results show that gal3-positive compartments get close to the plasma membrane, and that ALG2 plasma membrane recruitment in the same area subsequently occurs. This implies that the gal3-positive vesicles somehow trigger the ALG2 recruitment. However, the mechanism behind such a process remains unknown. It could be that the compartments physically poke a hole in the plasma membrane, which naturally would allow calcium influx at the site of rupture. This could be a random occurrence, or it could be controlled by a mechanism that forces the phagosomes towards the plasma membrane. It could also be that it is the bacteria and not the compartments that get in contact with the plasma membrane, and thereby trigger damage. Findings published by Conrad *et al.* in 2017 suggest that ESX-1-dependent membrane lysis is contact-dependent and results in large wounds rather than discrete pores [78]. The mechanism of the plasma membrane damage found here could be of the same nature. Whether or not the bacteria were close to the plasma membrane could have been more closely examined by looking at the eFluor 450 signal in TIRF mode. However, this was not feasible, as the fluorescent labeling was unpredictable and weak. Had the bacteria expressed fluorescent tags themselves, this problem could have been circumvented.

Another possibility is that there is some sort of signaling when the mycobacterium-containing compartments get close enough to the plasma membrane, inducing either damage, opening of calcium channels, formation of pores, or another process allowing calcium influx. Such a mechanism could be mediated by the bacterial ESX-1 secretion system, but the finding that nanosilica treatment results in the same characteristics suggests that physical contact resulting in a rupture is more likely. Furthermore, the observation that gal3-positive, LC3-positive vesicles get close to the plasma membrane without inducing an ALG2-response suggest that the autophagic mem-

brane somehow hinder the damage. These findings could perhaps be connected to ejection of bacteria, as discussed in more detail below.

There was a considerable amount of crosstalk between the gal3-mSc and the ALG2-mNG channels, as mScarlet gets some excitation from the 488 nm laser line, and the emission is allowed through the filter. This was not a big problem, as it was almost negligible in the TIRF channels, and it was circumvented in the AG cell line by having gal3 fused to SNAP instead of mScarlet. A linear unmixing algorithm plugin for FIJI was used to separate the channels in some cases, but seeing as the ALG2-mNG widefield channel was not the most interesting for the conclusions, the problem was not permanently solved. No ALG2 widefield accumulation events that could not be attributed to either crosstalk or plasma membrane recruitment were found, suggesting that endolysosomal repair is not primarily mediated by ALG2. This is in line with findings from Radulovic *et al.*, where TSG101 is identified as more prominent than ALIX in these cases [79]. However, Skowyra *et al.* has reported results that suggest a calcium-dependence for ESCRT recruitment in endomembrane repair, providing the opposite argument [80]. Evidently, the role of ALG2 is disputed in this regard.

The ALG2 plasma membrane recruitment events that were related to gal3-positive phagosomes were usually massive, local accumulations, accompanied by a later, weaker and transient even distribution of small ALG2 puncta. However, some ALG2 plasma membrane recruitment events were not related to a gal3-positive compartment and seemed to be related to a bacterium entering the cell. Furthermore, other ALG2-events were just an even recruitment into a starry pattern. A plausible scenario in the latter case is that a gal3-positive compartment gets close to the plasma membrane at the top of cell, resulting in a large, local ALG2 recruitment event there. Such a local ALG2 recruitment could also stem from phagocytosis of a bacterium. Subsequently, this local ALG2-event at the top of the cell could give an even ALG2 plasma membrane recruitment all over the plasma membrane, seen in the bottom as a the starry pattern. Thus, this could be the explanation for the transient and seemingly uncentered recruitment events.

Nevertheless, the cause of the small, transient puncta remains unknown. As ALG2 is recruited by calcium, it is likely that these puncta are sites of calcium influx at the plasma membrane, e.g. holes, pores or calcium channels. Each dot is seemingly stationary, supporting all these scenarios. A possible explanation could be that the bacteria cause a rupture in the membrane, which induces a massive, local ALG2 accumulation at the site of the bacteria/plasma membrane interface. This could then result in release of intracellular ATP, which subsequently binds to P2X7 receptors, giving a temporary calcium influx through channels, seen as the transient, even puncta pattern. This would explain why the large, local accumulation is observed before the more evenly distributed starry pattern, and why this starry pattern retracts (as the channels close). Such a scenario could possibly be seen in analysis of the Calbryte experiments, as

the influx through damage-inflicted plasma membrane openings seemed larger than channel-induced influx. Another possibility is that the smaller puncta are sites of GSDMD pores. The ALG2 recruitment could then be interpreted as ESCRT negatively regulating damage-induced pyroptosis, similar to mechanisms reported by Rühl *et al.* in 2018 [81]. However, our previous experiments with GSDMD knockdown cells displayed pre-speck membrane recruitment of ALG2 upon stimuli [8]. This suggests other mechanisms are important pre-speck, although mycobacterial infection was not tested. To elucidate the cause of the smaller ALG2 puncta, infection experiments in GSDMD knockdown cells or with calcium channel blockers present would be interesting.

Another important point of discussion is whether some gal3-events have a too low intensity or are too out of focus to measure or to see with the naked eye, as there are some ALG2-events that occur at sites of phagosomes that seem clearly negative. Such events could however possibly be explained by incomplete phagocytosis. Furthermore, some gal3-positive phagosomes lose their accumulated gal3 when an ALG2-event occur at the same site, from unknown reasons. All these situations could have been explored in greater detail by the use of correlative microscopy. To achieve this, one could use gridded wells and start by studying infected cells with TIRF. At the time of an ALG2 plasma membrane recruitment event, the well should be fixated with paraformaldehyde and washed with phosphate buffered saline. Thereafter, the same event can be traced back on the grid in another microscope, providing a greater resolution and thereby more information about the relative position of compartments and events.

5.3 Connections to autophagy

It is suggested in the results section that it is mostly gal3-positive, LC3B-negative compartments that result in an ALG2 recruitment event after the compartment gets close to the plasma membrane. However, the gray value measurements used for the quantification are affected by how some ROIs have to be quite large in order to fit the compartment through the relevant time of observation, since they move around to a great extent. The measured mean gray value could therefore be lower than it really is, because a lot of the background is included. Still, this effect should affect all measurements equally, and comparing the measurements is therefore nevertheless interesting. Furthermore, it could also be that some gal3-positive compartments are related to ALG2-events that happen after observation has stopped, and that they therefore are wrongly classified as unrelated to an ALG2 recruitment event. However, all measurements were aligned to the event of the compartment turning gal3-positive, and the fact that there is a significant difference between the categories suggests that this is a negligible problem.

To make the analysis of LC3B-recruitment quicker and less biased, a better approach than

drawing ROIs would be to use the bacteria as segmentation, create a mask from the result and subsequently use this to measure the mean gray value increase in the LC3B-channel. However, it was difficult to implement such a process: The bacteria was not evenly colored, as a dye was used instead of a genetic tag. Also, the bacteria drifted in and out of focus, as they are very small compared to the cells. A better approach to fluorescent labeling could solve this, for instance BFP-expressing bacteria. In future experiments, the labeling should be improved and a segmentation approach should be used for quantification. This could possibly also provide cleaner measurements with less uncertainty.

5.3.1 Host cell ejection of bacteria

As mentioned, the interplay between ALG2, gal3 and LC3B seen in the results could be connected to ejection of bacteria. A 2015 study by Miao *et al.* reported interesting results on this topic [82]. The authors found that uropathogenic *E. coli* are taken up in bladder epithelial cells, and eventually, they reach lysosomal compartments. Here, the bacteria neutralizes the pH. This event is sensed by lysosomal transient receptor potential (TRP) cation channels, which subsequently open and allow Ca^{2+} efflux. Finally, this triggers exocytosis of the lysosomal compartment, and the bacteria is released from the cell. The authors found that components from the autophagic machinery in the expelled compartments. Also, LC3-positive autophagosomes were frequently observed, and inducers of autophagy increased the amount of ejected bacteria, while knockdown of autophagy has the opposite result. This mechanism is possibly a form of secretory autophagy, and could be relevant also in the context of *Mtb* infection in macrophages. TRP channels could therefore be an interesting target to study in future experiments.

Furthermore, Hagedorn *et al.* in 2009 and the follow-up paper from Gerstenmaier *et al.* in 2015 provided new insights into spread of mycobacteria [83, 84]. The authors use a model system of *Mycobacterium marinum (M. marinum)* infection in the amoeba *Dictyostelium*. In the first study, they find that *Mtb* and *M. marinum* exit their host in an F-actin-based structure they term the ejectosome. These ejectosomes are short and barrel-shaped, unlike the long lamellipodia seen in the phagocytic process when the bacteria enters the amoeba. In the process of ejection, the bacteria breaches the plasma membrane, creating a hole, which is subsequently resealed. Evidently, such a mechanism could be relevant in the work presented here, and an approach that could have been tried to elucidate a connection to bacterial ejection is thus fluorescent labeling of actin. Furthermore, in the next study, Gerstenmaier *et al.* identify autophagy as an important player in the ejection process. By the use of correlative light electron microscopy, they conclude that Atg8 (the yeast homologue of LC3B) is recruited to a cup around the intracellular part of mycobacteria in the process of being ejected. This accumulation started very early, when the bacterium was still almost completely inside the cell, and stayed until it was

fully ejected.

Also, in late 2018, the same group published new research on this system in a paper by López-Jiménez *et al.* [85]. Here, they studied the interplay between the ESCRT system and autophagy at the site of *Mycobacterium*-containing compartments. Their findings support that ESX-1 mediated damage of the compartment itself is repaired by both machineries. However, when knocking out autophagy, the bacteria translocate from the phagosome to the cytosol earlier and proliferate in the cytosol. When knocking out ESCRT, on the other hand, there is an increased recruitment of autophagy proteins and ubiquitin when the phagosomal membrane is not repaired. This limits the growth of the bacteria. In light of these findings, the decreased recruitment of LC3B to gal3-positive, ALG2-related phagosomes could be explained by how an increase in ESCRT activity could be balanced by decrease in autophagy. However, the ESCRT recruitment mechanisms studied by López-Jiménez *et al.* differ from the ALG2-dependent route, limiting the relevance of these results.

Another interesting approach to this topic has been demonstrated by Czuczman *et al.* in 2014 and Tan *et al.* in 2018 [86, 87]. These studies look at cell-to-cell spread of *Listeria monocytogenes*, a bacterium that uses a pore-forming toxin to thrive and spread to new hosts. Here, they find that autophagy-related proteins ATG16L1, ATG5 and ATG12 are needed for plasma membrane repair. During ATG16L1 deficiency, however, ESCRT recruitment to the plasma membrane was seemingly unaffected, suggesting that these routes are independent. Furthermore, they find that LC3B is not recruited to the plasma membrane when it is damaged. In another, more recent study, ATG16L1 was found to be important for xenophagy processes [88]. Altogether, this too could suggest that the greater recruitment of LC3B to ALG2-unrelated compartments that is seen in the results is due to autophagy-mediated repair of the membrane, replacing the need for ESCRT. ATG16L1 is probably of greater importance than LC3B in such a scenario, supported by how the authors do not find LC3B at the plasma membrane during damage. Thus, a focus on ATG16L1 could be fruitful in future experimental endeavors concerning this system.

5.4 The role of ESCRT

Mittal *et al.* reported in late 2018 that the mycobacterial ESX-1 system and ESCRT proteins compete in trying to breach and repair the phagosomal membrane, respectively [89]. They use imaging to show that THP-1 cells infected with bacteria lacking the ESX-1 system, and uninfected cells, did not experience a significant change in the distribution of ESCRT proteins. THP-1 cells infected with bacteria with an intact ESX-1 system, on the other hand, responded with redistribution of the ESCRT proteins into a punctate pattern. Although this report does not address plasma membrane damage, the findings are nevertheless interesting in relation to the work de-

scribed in this thesis, as they show a link between ESCRT and pathogen-induced damage. This was also underlined in the above-mentioned study from López-Jimenez and colleagues [85], which show that ESCRT prevents phagosomal escape.

Furthermore, it has previously been shown that infection with *Mtb* causes small wounds in the plasma membrane, and that their repair through the lysosomal fusion route is inhibited [90]. This is in line with the notion that ESCRT is responsible for the repair of such damage. The previously mentioned study by Rühl *et al.* [81], identifying ESCRT as a negative regulator of pyroptosis post-GSDMD activation, clearly demonstrate that ESCRT and this particular death pathway have a connection.

All in all, ESCRT could be working to prevent *Mtb* spread both from the phagosomal escape perspective, as indicated in the literature, and possibly also in the setting of plasma membrane damage, as demonstrated in this thesis.

5.5 Calcium fluxes and their importance in NLRP3 activation

It is suggested by the results that ALG2 plasma membrane recruitment is associated with a calcium flux in the cell. However, this is not entirely proven to be influx of calcium from the extracellular environment, as no control experiment was done without calcium in the cell medium. Yet, ESCRT has been seen not to be recruited when there is no extracellular calcium [40], implying that such experiments would not yield any ALG2-events to examine. Furthermore, seeing as the recruitment happens locally at the plasma membrane, it is likely that the source of the calcium is the extracellular milieu. Nevertheless, experiments could have been done with ER calcium release inhibitors to exclude that the ER plays a role, which is conceivable, as it is situated close to the plasma membrane in some cases [91].

Furthermore, the temporal resolution in the Calbryte experiments is too poor to compare the initiation of the ALG2-events to the changes in Calbryte intensity in great detail. Here, rather than simply identifying the start point, the ALG2 plasma membrane recruitment could have been quantified. This quantification could have been correlated with the Calbryte gray value measurements, and more information could possibly be obtained. In the specialization project work, the machine-learning based program Ilastik was used for quantification of ALG2 plasma membrane recruitment [8]. However, this approach was not suitable in the more complex situation of an *Mtb* $mc^2$6206 infection with both large, local accumulations and smaller, transient puncta. Also, as the frames have 10 seconds between them due to the high number of channels, correlating Calbryte intensity changes with the quick ALG2 plasma membrane recruitment would possibly not change the quantification results significantly. For future reference, fewer channels and shorter frame intervals should be used, and the ALG2 plasma membrane recruit-

ment should be quantified. A greater temporal resolution could also reveal quicker Calbryte intensity changes.

In the quantification of the Calbryte experiments, the gray value seemingly decreases more for the cases of *Mtb* mc^{2}6206-mediated ALG2-events than for nanosilica-mediated ALG2-events. This could mean that calcium is pumped out of the cells at a faster rate during *Mtb* mc^{2}6206 infection as compared to during nanosilica treatment. Possibly, the response to a pathogenic infection results in a more active cellular response than sterile damage, but this could also be random, as the sample size is small.

5.5.1 Plasma membrane damage as a driver of NLRP3 activation

As was mentioned in the theory section, the role of ion fluxes in NLRP3 activation is a matter of great debate. There is consensus that induction of potassium efflux triggers NLRP3 activation, while there is more uncertainty tied to calcium influx. Furthermore, it is unclear exactly how *Mtb* activates the NLRP3 inflammasome [92]. Nevertheless, the ESX-1 system and ESAT-6 has been shown to be of importance for *Mtb*-induced NLRP3 activation, suggesting that membrane damage is central [93, 94].

In this work, it has been shown that calcium fluxes, most likely influx from the extracellular milieu, accompanies ALG2 plasma membrane recruitment. Such recruitment in many cases appear prior to NLRP3 activation: 9 out of 10 specks in cells stimulated with nanosilica came subsequent to an ALG2-event, while 17 out of 31 specks in cells infected with *Mtb* mc^{2}6206 were in a cell that had a pre-speck ALG2-event. Seemingly, there is a higher background speck formation in cells that are have pathogenic rather than sterile damage. Seeing as an infection is the more complex situation of the two, this is not surprising, as the bacteria probably inflict several other damaging effects upon the host cells, in addition to membrane damage. There could therefore be other mechanisms driving speck formation as well. Nevertheless, calcium influx likely occurs during damage to the plasma membrane, suggesting that a potassium efflux is present as well. Plasma membrane damage could thus be a driver for NLRP3 inflammasome activation in this setting.

Chapter 6

Conclusion and further work

In THP-1 cells, the response of fluorescently tagged membrane repair-associated protein ALG2, phagosomal escape marker gal3, NLRP3 inflammasome adapter protein ASC, and autophagy-related protein LC3B was recorded during treatment with nanosilica and infection with *Mtb* $mc^2$6206 by using TIRF microscopy. It was found that ALG2 recruitment to the plasma membrane frequently occurs in large, local accumulations positioned close to gal3-positive compartments. Furthermore, autophagy machinery was found to be recruited to gal3-positive compartments. Seemingly, this was a more prominent feature for compartments that were related to ALG2-events. However, delay of the autophagy onset by the use of an inhibitor did not affect ALG2 plasma membrane recruitment events. Lastly, it was found that ALG2 recruitment to the plasma membrane is associated with a calcium flux, while the recruitment of gal3 to breached phagosomal compartments is not.

To elucidate further the exact mechanisms of the system, correlative microscopy should be carried out, increasing both resolution and spatial information. This should include both high-resolution light microscopy techniques such as confocal microscopy and various superresolution techniques, and electron microscopy. Such experiments could reveal ultrastructural information to help understand the mechanisms of the system, for instance with regard to whether or not the interaction between the mycobacterium-containing compartment and the plasma membrane is contact-dependent or not.

Additionally, autophagic protein knockout cell lines should be explored further to establish the role of autophagy processes. Furthermore, to examine relations to bacterial ejection, actin, TRP channels and ATG16L1 should be studied in this system. Also, Calbryte experiments with an ER calcium release inhibitor present should be conducted to verify that it is most likely extracellular calcium that enters the cell during ALG2 events.

In summary, this research shows promise in uncovering molecular details of early stages in *Mtb* infection, which could be of relevance in future endeavors to control tuberculosis.

Bibliography

[1] Geneva: World Health Organization. *Global tuberculosis report 2018*. World Health Organization, 2018. Licence: CC BY-NC-SA 3.0 IGO.

[2] D. L. Clemens and M. A. Horwitz. Characterization of the *Mycobacterium tuberculosis* phagosome and evidence that phagosomal maturation is inhibited. *Journal of Experimental Medicine*, 181(1):257–270, 1995. ISSN 0022-1007. doi: 10.1084/jem.181.1.257.

[3] Diane Houben, Caroline Demangel, Jakko van Ingen, Jorge Perez, Lucy Baldeón, Abdallah M. Abdallah, Laxmee Caleechurn, Daria Bottai, Maaike van Zon, Karin de Punder, Tridia van der Laan, Arie Kant, Ruth Bossers-de Vries, Peter Willemsen, Wilbert Bitter, Dick van Soolingen, Roland Brosch, Nicole van der Wel, and Peter J. Peters. ESX-1-mediated translocation to the cytosol controls virulence of mycobacteria. *Cellular Microbiology*, 14(8):1287–1298, 2012. doi: 10.1111/j.1462-5822.2012.01799.x.

[4] Maximiliano G. Gutierrez, Sharon S. Master, Sudha B. Singh, Gregory A. Taylor, Maria I. Colombo, and Vojo Deretic. Autophagy Is a Defense Mechanism Inhibiting BCG and *Mycobacterium tuberculosis* Survival in Infected Macrophages. *Cell*, 119(6):753–766, 2004. ISSN 0092-8674. doi: 10.1016/j.cell.2004.11.038.

[5] Anca Dorhoi, Geraldine Nouailles, Sabine Jörg, Kristine Hagens, Ellen Heinemann, Lydia Pradl, Dagmar Oberbeck-Müller, Maria Adelaida Duque-Correa, Stephen T. Reece, Jürgen Ruland, Roland Brosch, Jürg Tschopp, Olaf Gross, and Stefan H. E. Kaufmann. Activation of the NLRP3 inflammasome by *Mycobacterium tuberculosis* is uncoupled from susceptibility to active tuberculosis. *European Journal of Immunology*, 42(2):374–384, 2012. doi: 10.1002/eji.201141548.

[6] James W. Pinkerton, Richard Y. Kim, Avril A.B. Robertson, Jeremy A. Hirota, Lisa G. Wood, Darryl A. Knight, Matthew A. Cooper, Luke A.J. O'Neill, Jay C. Horvat, and Philip M. Hansbro. Inflammasomes in the lung. *Molecular Immunology*, 86:44–55, 2017. ISSN 0161-5890. doi: 10.1016/j.molimm.2017.01.014.

[7] Ana Joaquina Jimenez, Paolo Maiuri, Julie Lafaurie-Janvore, Séverine Divoux, Matthieu Piel, and Franck Perez. ESCRT Machinery Is Required for Plasma Membrane Repair. *Science*, 343(6174), 2014. ISSN 0036-8075. doi: 10.1126/science.1247136.

[8] Ragnhild Sofie Ragnhildstveit Sætra. Investigating plasma membrane damage during NLRP3 inflammasome activation. Unpublished specialization project report, NTNU, December 2018.

[9] Harvey Lodish, Arnold Berk, Chris A. Kaiser, Monty Krieger, Anthony Bretscher, Hidde Ploegh, Angelike Amon, and Kelsey C. Martin. *Molecular Cell Biology*. W. H. Freeman, 8th edition, 2016. ISBN 978-1-4641-8339-3.

[10] Geoffrey M. Cooper and Robert E. Hausman. *The Cell: A Molecular Approach*. Sinauer Associates, Inc., 6th edition, 2013. ISBN 978-0-87893-964-0.

[11] Cuiping Pan, Chanchal Kumar, Sebastian Bohl, Ursula Klingmueller, and Matthias Mann. Comparative Proteomic Phenotyping of Cell Lines and Primary Cells to Assess Preservation of Cell Type-specific Functions. *Molecular & Cellular Proteomics*, 8(3):443–450, 2009. ISSN 1535-9476. doi: 10.1074/mcp.M800258-MCP200.

[12] Jeff Hardin and Gregory Bertoni. *Becker's World of the Cell*. Pearson Education Ltd, 9th edition, 2018. ISBN 978-1-292-17769-4.

[13] Martin Jinek, Krzysztof Chylinski, Ines Fonfara, Michael Hauer, Jennifer A. Doudna, and Emmanuelle Charpentier. A Programmable Dual-RNA–Guided DNA Endonuclease in Adaptive Bacterial Immunity. *Science*, 337(6096):816–821, 2012. ISSN 0036-8075. doi: 10.1126/science.1225829.

[14] Giedrius Gasiunas, Rodolphe Barrangou, Philippe Horvath, and Virginijus Siksnys. Cas9–crRNA ribonucleoprotein complex mediates specific DNA cleavage for adaptive immunity in bacteria. *Proceedings of the National Academy of Sciences*, 109(39):E2579–E2586, 2012. ISSN 0027-8424. doi: 10.1073/pnas.1208507109.

[15] Jason D. Simmons, Catherine M. Stein, Chetan Seshadri, Monica Campo, Galit Alter, Sarah Fortune, Erwin Schurr, Robert S. Wallis, Gavin Churchyard, Harriet Mayanja-Kizza, W. Henry Boom, and Thomas R. Hawn. Immunological mechanisms of human resistance to persistent Mycobacterium tuberculosis infection. *Nature Reviews Immunology*, 18:1–15, 2018. ISSN 14741741. doi: 10.1038/s41577-018-0025-3.

[16] Chelsea E. Stamm, Angela C. Collins, and Michael U. Shiloh. Sensing of *Mycobacterium tuberculosis* and consequences to both host and bacillus. *Immunological Reviews*, 264(1): 204–219, 2015. ISSN 1600065X. doi: 10.1111/imr.12263.

[17] Qiyao Chai, Yong Zhang, and Cui Hua Liu. *Mycobacterium tuberculosis*: An Adaptable Pathogen Associated With Multiple Human Diseases. *Frontiers in Cellular and Infection Microbiology*, 8(158):1–15, 2018. doi: 10.3389/fcimb.2018.00158.

[18] Kenneth Murphy and Casey Weaver. *Janeway's Immunobiology*. Garland Science, 9th edition, 2017. ISBN 978-0-8153-4505-3.

[19] Jane Atesoh Awuh and Trude Helen Flo. Molecular basis of mycobacterial survival in macrophages. *Cellular and Molecular Life Sciences*, 74:1625–1648, 2017. ISSN 1420-9071. doi: 10.1007/s00018-016-2422-8.

[20] Nicole van der Wel, David Hava, Diane Houben, Donna Fluitsma, Maaike van Zon, Jason Pierson, Michael Brenner, and Peter J. Peters. *M. tuberculosis* and *M. leprae* Translocate from the Phagolysosome to the Cytosol in Myeloid Cells. *Cell*, 129(7):1287–1298, 2007. ISSN 0092-8674. doi: 10.1016/j.cell.2007.05.059.

[21] Wandy L. Beatty, Elizabeth R. Rhoades, Daniel K. Hsu, Fu-Tong Liu, and David G. Russell. Association of a macrophage galactoside-binding protein with Mycobacterium-containing phagosomes. *Cellular Microbiology*, 4(3):167–176, 2002. doi: 10.1046/j.1462-5822.2002.00183.x.

[22] Irit Paz, Martin Sachse, Nicolas Dupont, Joelle Mounier, Cecilia Cederfur, Jost Enninga, Hakon Leffler, Francoise Poirier, Marie-Christine Prevost, Frank Lafont, and Philippe Sansonetti. Galectin-3, a marker for vacuole lysis by invasive pathogens. *Cellular Microbiology*, 12(4):530–544, 2010. doi: 10.1111/j.1462-5822.2009.01415.x.

[23] Hexin Shi, Ying Wang, Xiaohong Li, Xiaoming Zhan, Miao Tang, Maggy Fina, Lijing Su, David Pratt, Chun Hui Bu, Sara Hildebrand, Stephen Lyon, Lindsay Scott, Jiexia Quan, Qihua Sun, Jamie Russell, Stephanie Arnett, Peter Jurek, Ding Chen, Vladimir V. Kravchenko, John C. Mathison, Eva Marie Y. Moresco, Nancy L. Monson, Richard J. Ulevitch, and Bruce Beutler. NLRP3 activation and mitosis are mutually exclusive events coordinated by NEK7, a new inflammasome component. *Nature Immunology*, 17(3):250–258, 2016. ISSN 15292916. doi: 10.1038/ni.3333.

[24] Yuan He, Melody Y. Zeng, Dahai Yang, Benny Motro, and Gabriel Núñez. NEK7 is an essential mediator of NLRP3 activation downstream of potassium efflux. *Nature*, 530(7590): 354–357, 2016. ISSN 14764687. doi: 10.1038/nature16959.

[25] Andrea Stutz, Gabor L. Horvath, Brian G. Monks, and Eicke Latz. ASC Speck Formation as a Readout for Inflammasome Activation. In Christine M. De Nardo and Eicke Latz, editors, *The Inflammasome: Methods and Protocols*, pages 91–101. Humana Press, Totowa, NJ, 2013. ISBN 978-1-62703-523-1. doi: 10.1007/978-1-62703-523-1_8.

[26] Rongbin Zhou, Amir S. Yazdi, Philippe Menu, and Jürg Tschopp. A role for mitochondria in NLRP3 inflammasome activation. *Nature*, 469(7329):221–226, 2011. ISSN 00280836. doi: 10.1038/nature09663.

[27] Zhenyu Zhong, Shuang Liang, Elsa Sanchez-Lopez, Feng He, Shabnam Shalapour, Xue jia Lin, Jerry Wong, Siyuan Ding, Ekihiro Seki, Bernd Schnabl, Andrea L. Hevener, Harry B. Greenberg, Tatiana Kisseleva, and Michael Karin. New mitochondrial DNA synthesis enables NLRP3 inflammasome activation. *Nature*, 560(7717):198–203, 2018. ISSN 14764687. doi: 10.1038/s41586-018-0372-z.

[28] Jueqi Chen and Zhijian J. Chen. PtdIns4P on dispersed trans-Golgi network mediates NLRP3 inflammasome activation. *Nature*, 564(7734):71–76, 2018. ISSN 0028-0836. doi: 10.1038/s41586-018-0761-3.

[29] T. Murakami, J. Ockinger, J. Yu, V. Byles, A. McColl, A. M. Hofer, and T. Horng. Critical role for calcium mobilization in activation of the NLRP3 inflammasome. *Proceedings of the National Academy of Sciences*, 109(28):11282–11287, 2012. ISSN 0027-8424. doi: 10.1073/pnas.1117765109.

[30] Kathy Triantafilou, Timothy R. Hughes, Martha Triantafilou, and B. Paul Morgan. The complement membrane attack complex triggers intracellular Ca^{2+} fluxes leading to NLRP3 inflammasome activation. *Journal of Cell Science*, 2013. ISSN 0021-9533. doi: 10.1242/jcs.124388.

[31] J. R. Yaron, S. Gangaraju, M. Y. Rao, X. Kong, L. Zhang, F. Su, Y. Tian, H. L. Glenn, and D. R. Meldrum. K^+ regulates Ca^{2+} to drive inflammasome signaling: Dynamic visualization of ion flux in live cells. *Cell Death and Disease*, 6(10):1–11, 2015. ISSN 20414889. doi: 10.1038/cddis.2015.277.

[32] Masahiro Okada, Atsushi Matsuzawa, Akihiko Yoshimura, and Hidenori Ichijo. The lysosome rupture-activated TAK1-JNK pathway regulates NLRP3 inflammasome activation.

Journal of Biological Chemistry, 289(47):32926–32936, 2014. ISSN 1083351X. doi: 10.1074/jbc.M114.579961.

[33] Hao Chen, Dahai Yang, Fajun Han, Jinchao Tan, Lingzhi Zhang, Jingfan Xiao, Yuanxing Zhang, and Qin Liu. The Bacterial T6SS Effector EvpP Prevents NLRP3 Inflammasome Activation by Inhibiting the Ca^{2+}-Dependent MAPK-Jnk Pathway. *Cell Host & Microbe*, 21(1): 47–58, 2017. ISSN 1931-3128. doi: 10.1016/j.chom.2016.12.004.

[34] Michael A. Katsnelson, L. Graham Rucker, Hana M. Russo, and George R. Dubyak. K^+ Efflux Agonists Induce NLRP3 Inflammasome Activation Independently of Ca^{2+} Signaling. *The Journal of Immunology*, 194(8):3937–3952, 2015. ISSN 0022-1767. doi: 10.4049/jimmunol.1402658.

[35] Alex G. Baldwin, Jack Rivers-Auty, Michael J.D. Daniels, Claire S. White, Carl H. Schwalbe, Tom Schilling, Halah Hammadi, Panichakorn Jaiyong, Nicholas G. Spencer, Hazel England, Nadia M. Luheshi, Manikandan Kadirvel, Catherine B. Lawrence, Nancy J. Rothwell, Michael K. Harte, Richard A. Bryce, Stuart M. Allan, Claudia Eder, Sally Freeman, and David Brough. Boron-Based Inhibitors of the NLRP3 Inflammasome. *Cell Chem Biol.*, 24(11): 1321–1335.e5, 2017. doi: 10.1016/j.chembiol.2017.08.011.

[36] Xing Liu, Zhibin Zhang, Jianbin Ruan, Youdong Pan, Venkat Giri Magupalli, Hao Wu, and Judy Lieberman. Inflammasome-activated gasdermin D causes pyroptosis by forming membrane pores. *Nature*, 535(7610):153–158, 2016. ISSN 14764687. doi: 10.1038/nature18629.

[37] Jianjin Shi, Wenqing Gao, and Feng Shao. Pyroptosis: Gasdermin-Mediated Programmed Necrotic Cell Death. *Trends in Biochemical Sciences*, 42(4):245–254, 2017. ISSN 13624326. doi: 10.1016/j.tibs.2016.10.004.

[38] N. W. Andrews, M. Corrotte, and T. Castro-Gomes. Above the fray: Surface remodeling by secreted lysosomal enzymes leads to endocytosis-mediated plasma membrane repair. *Seminars in Cell & Developmental Biology*, 45:10–17, 2015. ISSN 1084-9521. doi: 10.1016/j.semcdb.2015.09.022.

[39] Norma W. Andrews and Matthias Corrotte. Plasma membrane repair. *Current Biology*, 28 (8):R392–R397, 2018. ISSN 09609822. doi: 10.1016/j.cub.2017.12.034.

[40] Luana L. Scheffer, Sen Chandra Sreetama, Nimisha Sharma, Sushma Medikayala, Kristy J. Brown, Aurelia Defour, and Jyoti K. Jaiswal. Mechanism of Ca^{2+}-triggered ESCRT assem-

bly and regulation of cell membrane repair. *Nature Communications*, 5:5646, 2014. ISSN 20411723. doi: 10.1038/ncomms6646.

[41] Jeff Hardin and Gregory Bertoni. *Becker's World of the Cell*. Pearson Education Ltd, 9th edition, 2018. ISBN 978-1-292-17769-4.

[42] Sebastian Alers, Antje S. Löffler, Sebastian Wesselborg, and Björn Stork. Role of AMPK-mTOR-Ulk1/2 in the Regulation of Autophagy: Cross Talk, Shortcuts, and Feedbacks. *Molecular and Cellular Biology*, 32(1):2–11, 2012. doi: 10.1128/MCB.06159-11.

[43] Maria Zachari and Ian G. Ganley. The mammalian ULK1 complex and autophagy initiation. *Essays in Biochemistry*, 61(6):585–596, 2017. doi: 10.1042/EBC20170021.

[44] Sebastian Wesselborg and Björn Stork. Autophagy signal transduction by ATG proteins: from hierarchies to networks. *Cellular and Molecular Life Sciences*, 72:4721–4757, 2015. doi: 10.1007/s00018-015-2034-8.

[45] Julia Dancourt and Thomas J Melia. Lipidation of the autophagy proteins LC3 and GABARAP is a membrane-curvature dependent process. *Autophagy*, 10(8):1470–1471, 2014. doi: 10.4161/auto.29468.

[46] You-Kyung Lee and Jin-A Lee. Role of the mammalian ATG8/LC3 family in autophagy: differential and compensatory roles in the spatiotemporal regulation of autophagy. *BMB Reports*, 49(8):424–430, 2016. doi: 10.5483/BMBRep.2016.49.8.081.

[47] Robert O. Watson, Paolo S. Manzanillo, and Jeffery S. Cox. Extracellular *M. tuberculosis* DNA Targets Bacteria for Autophagy by Activating the Host DNA-Sensing Pathway. *Cell*, 150(4):803–815, 2012. ISSN 0092-8674. doi: 10.1016/j.cell.2012.06.040.

[48] Robert O. Watson, Samantha L. Bell, Donna A. MacDuff, Jacqueline M. Kimmey, Elie J. Diner, Joanna Olivas, Russell E. Vance, Christina L. Stallings, Herbert W. Virgin, and Jeffery S. Cox. The cytosolic sensor cGAS detects *Mycobacteirum tuberculosis* DNA to induce type I interferons and activate autophagy. *Cell Host & Microbe*, 17(6):811–819, 2015. doi: 10.1016/j.chom.2015.05.004.

[49] Paolo S. Manzanillo, Janelle S. Ayres, Robert O. Watson, Angela C. Collins, Gianne Souza, Chris S. Rae, David S. Schneider, Ken Nakamura, Michael U. Shiloh, and Jeffery S. Cox. The ubiquitin ligase parkin mediates resistance to intracellular pathogens. *Nature*, 501(7468):512–516, 2013. ISSN 0028-0836. doi: 10.1038/nature12566. URL 10.1038/nature12566.

[50] Luis H. Franco, Vidhya R. Nair, Caitlyn R. Scharn, Ramnik J. Xavier, Jose R. Torrealba, Michael U. Shiloh, and Beth Levine. The ubiquitin-ligase Smurf1 functions in selective autophagy of *M. tuberculosis* and anti-tuberculosis host defense. *Cell Host & Microbe*, 21 (1):59–72, 2017. doi: 10.1016/j.chom.2016.11.002.

[51] Bradlee L. Heckmann and Douglas R. Green. LC3-associated phagocytosis at a glance. *Journal of Cell Science*, 132(5), 2019. ISSN 0021-9533. doi: 10.1242/jcs.222984.

[52] Shu-chin Lai and Rodney J. Devenish. LC3-Associated Phagocytosis (LAP): Connections with Host Autophagy. *Cells*, 1(3):396–408, 2012. doi: 10.3390/cells1030396.

[53] Grace Y. Lam, Marija Cemma, Aleixo M. Muise, Darren E. Higgins, and John H. Brumell. Host and bacterial factors that regulate LC3 recruitment to *Listeria monocytogenes* during the early stages of macrophage infection. *Autophagy*, 9(7):985–995, 2013. doi: 10.4161/auto.24406.

[54] Tomonori Kimura, Jingyue Jia, Aurore Claude-Taupin, Suresh Kumar, Seong Won Choi, Yuexi Gu, Michal Mudd, Nicolas Dupont, Shanya Jiang, Ryan Peters, Farzin Farzam, Ashish Jain, Keith A. Lidke, Christopher M. Adams, Terje Johansen, and Vojo Deretic. Cellular and molecular mechanism for secretory autophagy. *Autophagy*, 13(6):1084–1085, 2017. ISSN 1554-8627. doi: 10.1080/15548627.2017.1307486.

[55] Marisa Ponpuak, Michael A. Mandell, Tomonori Kimura, Santosh Chauhan, Cédric Cleyrat, and Vojo Deretic. Secretory autophagy. *Current Opinion in Cell Biology*, 35:106–116, 2015. ISSN 0955-0674. doi: 10.1016/j.ceb.2015.04.016.

[56] Juhyung Lee and Yihong Ye. The Roles of Endo-Lysosomes in Unconventional Protein Secretion. *Cells*, 7(11), 2018. ISSN 2073-4409. doi: 10.3390/cells7110198.

[57] Caroline Bruns, J. Michael McCaffery, Amy J. Curwin, Juan M. Duran, and Vivek Malhotra. Biogenesis of a novel compartment for autophagosome-mediated unconventional protein secretion. *The Journal of Cell Biology*, 195(6):979–992, 2011. ISSN 0021-9525. doi: 10.1083/jcb.201106098.

[58] Paras N. Prasad. *Introduction to Biophotonics*. John Wiley and Sons, Inc., 1st edition, 2003. ISBN 0-471-28770-9.

[59] Juan Carlos Stockert and Alfonso Blázquez-Castro. *Fluorescence Microscopy in Life Sciences*. Bentham Sciences, 2017. ISBN 978-1-68108-518-0.

[60] M. Chalfie, Y. Tu, G. Euskirchen, W. W. Ward, and D. C. Prasher. Green fluorescent protein as a marker for gene expression. *Science*, 263(5148):802–805, 1994. ISSN 0036-8075. doi: 10.1126/science.8303295.

[61] Ben N. G. Giepmans, Stephen R. Adams, Mark H. Ellisman, and Roger Y. Tsien. The Fluorescent Toolbox for Assessing Protein Location and Function. *Science*, 312(5771):217–224, 2006. ISSN 0036-8075. doi: 10.1126/science.1124618.

[62] Melanie M. Frigault, Judith Lacoste, Jody L. Swift, and Claire M. Brown. Live-cell microscopy – tips and tools. *Journal of Cell Science*, 122(6):753–767, 2009. ISSN 0021-9533. doi: 10.1242/jcs.033837.

[63] M. L. Martin-Fernandez, C. J. Tynan, and S. E. D. Webb. A 'pocket guide' to total internal reflection fluorescence. *Journal of Microscopy*, 252(1):16–22, 2013. doi: 10.1111/jmi.12070.

[64] Alexa L. Mattheyses, Sanford M. Simon, and Joshua Z. Rappoport. Imaging with total internal reflection fluorescence microscopy for the cell biologist. *Journal of Cell Science*, 123 (21):3621–3628, 2010. doi: 10.1242/jcs.056218.

[65] Daniel Axelrod. Evanescent Excitation and Emission in Fluorescence Microscopy. *Biophysical Journal*, 104(7):1401–1409, 2013. ISSN 0006-3495. doi: 10.1016/j.bpj.2013.02.044.

[66] Shigeru Tsuchiya, Michiko Yamabe, Yoshiko Yamaguchi, Yasuko Kobayashi, Tasuke Konno, and Keiya Tada. Establishment and characterization of a human acute monocytic leukemia cell line (THP-1). *International Journal of Cancer*, 26(2):171–176, 1980. doi: 10.1002/ijc.2910260208.

[67] Nathan C. Shaner, Gerard G. Lambert, Andrew Chammas, Yuhui Ni, Paula J. Cranfill, Michelle A. Baird, Brittney R. Sell, John R. Allen, Richard N. Day, Maria Israelsson, Michael W. Davidson, and Jiwu Wang. A bright monomeric green fluorescent protein derived from Branchiostoma lanceolatum. *Nature Methods*, 10(5):407–409, 2013. ISSN 15487091. doi: 10.1038/nmeth.2413.

[68] Daphne S. Bindels, Lindsay Haarbosch, Laura Van Weeren, Marten Postma, Katrin E. Wiese, Marieke Mastop, Sylvain Aumonier, Guillaume Gotthard, Antoine Royant, Mark A. Hink, and Theodorus W.J. Gadella. mScarlet: A bright monomeric red fluorescent protein for cellular imaging. *Nature Methods*, 14(1):53–56, 2016. ISSN 15487105. doi: 10.1038/nmeth.4074.

[69] Grigory S. Filonov, Kiryl D. Piatkevich, Li Min Ting, Jinghang Zhang, Kami Kim, and Vladislav V. Verkhusha. Bright and stable near-infrared fluorescent protein for in vivo imaging. *Nature Biotechnology*, 29(8):757–761, 2011. ISSN 10870156. doi: 10.1038/nbt.1918.

[70] Antje Keppler, Susanne Gendreizig, Thomas Gronemeyer, Horst Pick, Horst Vogel, and Kai Johnsson. A general method for the covalent labeling of fusion proteins with small molecules in vivo. *Nature Biotechnology*, 21:86–89, 2003. doi: 10.1038/nbt765.

[71] Samantha L. Sampson, Christopher C. Dascher, Vasan K. Sambandamurthy, Robert G. Russell, William R. Jacobs, Barry R. Bloom, and Mary K. Hondalus. Protection Elicited by a Double Leucine and Pantothenate Auxotroph of Mycobacterium tuberculosis in Guinea Pigs. *Infection and Immunity*, 72(5):3031–3037, 2004. doi: 10.1128/IAI.72.5.3031.

[72] Katy J. Petherick, Owen J. L. Conway, Chido Mpamhanga, Simon A. Osborne, Ahmad Kamal, Barbara Saxty, and Ian G. Ganley. Pharmacological Inhibition of ULK1 Kinase Blocks Mammalian Target of Rapamycin (mTOR)-dependent Autophagy. *Journal of Biological Chemistry*, 290(18):11376–11383, 2015. doi: 10.1074/jbc.C114.627778.

[73] Johannes Schindelin, Ignacio Arganda-Carreras, Erwin Frise, Verena Kaynig, Mark Longair, Tobias Pietzsch, Stephan Preibisch, Curtis Rueden, Stephan Saalfeld, Benjamin Schmid, Jean Yves Tinevez, Daniel James White, Volker Hartenstein, Kevin Eliceiri, Pavel Tomancak, and Albert Cardona. Fiji: An open-source platform for biological-image analysis. *Nature Methods*, 9(7):676–682, 2012. ISSN 15487091. doi: 10.1038/nmeth.2019.

[74] Mann Whitney U-test Calculator. http://scistatcalc.blogspot.com/2013/10/mann-whitney-u-test-calculator.html. Accessed: 2019-05-07.

[75] R. Alan North. Molecular Physiology of P2X Receptors. *Physiological Reviews*, 82(4):1013–1067, 2002. doi: 10.1152/physrev.00015.2002. PMID: 12270951.

[76] Irma Podolak, Agnieszka Galanty, and Danuta Sobolewska. Saponins as cytotoxic agents: a review. *Phytochem Rev*, 9:425–474, 2010. doi: 10.1007/s11101-010-9183-z.

[77] Kristian Berg, Solveig Nordstrand, Pål Kristian Selbo, Diem Thuy Thi Tran, Even Angell-Petersen, and Anders Høgset. Disulfonated tetraphenyl chlorin (TPCS2a), a novel photosensitizer developed for clinical utilization of photochemical internalization. *Photochem. Photobiol. Sci.*, 10(10):1637–1651, 2011. doi: 10.1039/C1PP05128H.

[78] William H. Conrad, Morwan M. Osman, Jonathan K. Shanahan, Frances Chu, Kevin K. Takaki, James Cameron, Digby Hopkinson-Woolley, Roland Brosch, and Lalita Ramakrishnan. Mycobacterial ESX-1 secretion system mediates host cell lysis through bacterium

contact-dependent gross membrane disruptions. *Proceedings of the National Academy of Sciences*, 114(6):1371–1376, 2017. ISSN 0027-8424. doi: 10.1073/pnas.1620133114.

[79] Maja Radulovic, Kay O Schink, Eva M Wenzel, Viola Nähse, Antonino Bongiovanni, Frank Lafont, and Harald Stenmark. ESCRT-mediated lysosome repair precedes lysophagy and promotes cell survival. *The EMBO Journal*, 37(21), 2018. ISSN 0261-4189. doi: 10.15252/embj.201899753.

[80] Michael L. Skowyra, Paul H. Schlesinger, Teresa V. Naismith, and Phyllis I. Hanson. Triggered recruitment of ESCRT machinery promotes endolysosomal repair. *Science*, 360 (6384), 2018. ISSN 0036-8075. doi: 10.1126/science.aar5078.

[81] Sebastian Rühl, Kateryna Shkarina, Benjamin Demarco, Rosalie Heilig, José Carlos Santos, and Petr Broz. ESCRT-dependent membrane repair negatively regulates pyroptosis downstream of GSDMD activation. *Science*, 362(6417):956–960, 2018. ISSN 0036-8075. doi: 10.1126/science.aar7607.

[82] Yuxuan Miao, Guojie Li, Xiaoli Zhang, Haoxing Xu, and Soman N Abraham. A TRP Channel Senses Lysosome Neutralization by Pathogens to Trigger Their Expulsion Article A TRP Channel Senses Lysosome Neutralization by Pathogens to Trigger Their Expulsion. *Cell*, 161(6):1306–1319, 2015. ISSN 0092-8674. doi: 10.1016/j.cell.2015.05.009.

[83] Monica Hagedorn, Kyle H. Rohde, David G. Russell, and Thierry Soldati. Infection by Tubercular Mycobacteria Is Spread by Nonlytic Ejection from Their Amoeba Hosts. *Science*, 323(5922):1729–1733, 2009. ISSN 0036-8075. doi: 10.1126/science.1169381.

[84] Lilli Gerstenmaier, Rachel Pilla, Lydia Herrmann, Hendrik Herrmann, Monica Prado, Geno J. Villafano, Margot Kolonko, Rudolph Reimer, Thierry Soldati, Jason S. King, and Monica Hagedorn. The autophagic machinery ensures nonlytic transmission of mycobacteria. *Proceedings of the National Academy of Sciences*, 112(7):E687–E692, 2015. ISSN 0027-8424. doi: 10.1073/pnas.1423318112.

[85] Ana T. López-Jiménez, Elena Cardenal-Muñoz, Florence Leuba, Lilli Gerstenmaier, Caroline Barisch, Monica Hagedorn, Jason S. King, and Thierry Soldati. The ESCRT and autophagy machineries cooperate to repair ESX-1-dependent damage at the *Mycobacterium*-containing vacuole but have opposite impact on containing the infection. *PLOS Pathogens*, 14(12):1–29, 12 2019. doi: 10.1371/journal.ppat.1007501.

[86] Mark A. Czuczman, Ramzi Fattouh, Jorik M. Van Rijn, Veronica Canadien, Suzanne Osborne, Aleixo M. Muise, Vijay K. Kuchroo, Darren E. Higgins, and John H. Brumell. *Liste-*

ria monocytogenes exploits efferocytosis to promote cell-to-cell spread. *Nature*, 509(7499): 230–234, 2014. ISSN 0028-0836. doi: 10.1038/nature13168.

[87] Joel M. J. Tan, Nora Mellouk, Suzanne E. Osborne, Dustin A. Ammendolia, Diana N. Dyer, Ren Li, Diede Brunen, Jorik M. Van Rijn, Ju Huang, Mark A. Czuczman, Marija A. Cemma, Amy M. Won, Christopher M. Yip, Ramnik J. Xavier, Donna A. Macduff, Fulvio Reggiori, Jayanta Debnath, Tamotsu Yoshimori, Peter K. Kim, Gregory D. Fairn, Etienne Coyaud, Brian Raught, Aleixo M. Muise, Darren E. Higgins, and John H. Brumell. An ATG16L1-dependent pathway promotes plasma membrane repair and limits *Listeria monocytogenes* cell-to-cell spread. *Nature Microbiology*, 3:1472–1485, 2018. ISSN 2058-5276. doi: 10.1038/s41564-018-0293-5.

[88] Reham M Alsaadi, Truc T Losier, Wensheng Tian, Anne Jackson, Zhihao Guo, David C Rubinsztein, and Ryan C Russell. ULK1-mediated phosphorylation of ATG16L1 promotes xenophagy, but destabilizes the ATG16L1 Crohn's mutant. *EMBO reports*, 2019. ISSN 1469-221X. doi: 10.15252/embr.201846885.

[89] Ekansh Mittal, Michael L. Skowyra, Grace Uwase, Emir Tinaztepe, Alka Mehra, Stefan Köster, Phyllis I. Hanson, and Jennifer A. Philips. *Mycobacterium tuberculosis* Type VII Secretion System Effectors Differentially Impact the ESCRT Endomembrane Damage Response. *mBio*, 9(6):e01765–18, 2018. doi: 10.1128/mBio.01765-18.

[90] Maziar Divangahi, Minjian Chen, Huixian Gan, Danielle Desjardins, Tyler T Hickman, David M Lee, Sarah Fortune, Samuel M Behar, and Heinz G Remold. *Mycobacterium tuberculosis* evades macrophage defenses by inhibiting plasma membrane repair. *Nature Immunology*, 10(8):899–906, 2009. ISSN 1529-2908. doi: 10.1038/ni.1758.

[91] Emmanuel Okeke, Hayley Dingsdale, Tony Parker, Svetlana Voronina, and Alexei V. Tepikin. Endoplasmic reticulum–plasma membrane junctions: structure, function and dynamics. *The Journal of Physiology*, 594(11):2837–2847, 2016. doi: 10.1113/JP271142.

[92] Ka-Wing Wong. The Role of ESX-1 in *Mycobacterium tuberculosis* Pathogenesis. *Microbiology Spectrum*, 5(3):TBTB2–0001–2015, 2017. doi: 10.1128/microbiolspec.TBTB2-0001-2015.

[93] Bibhuti B. Mishra, Pedro Moura-Alves, Avinash Sonawane, Nir Hacohen, Gareth Griffiths, Luis F. Moita, and Elsa Anes. *Mycobacterium tuberculosis* protein ESAT-6 is a potent activator of the NLRP3/ASC inflammasome. *Cellular Microbiology*, 12(8):1046–1063, 2010. doi: 10.1111/j.1462-5822.2010.01450.x.

[94] Hana Abdalla, Lalitha Srinivasan, Swati Shah, Katrin D. Mayer-Barber, Alan Sher, Fayyaz S. Sutterwala, and Volker Briken. *Mycobacterium tuberculosis* Infection of Dendritic Cells Leads to Partially Caspase-1/11-Independent IL-1β and IL-18 Secretion but Not to Pyroptosis. *PLOS ONE*, 7(7):1–10, 07 2012. doi: 10.1371/journal.pone.0040722.